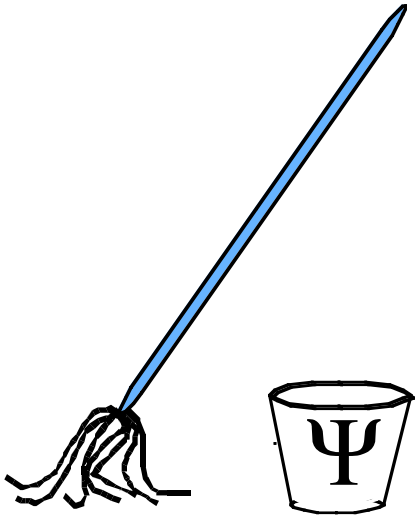

QM for AMOP

Chapter 9

Time Evolution and Fourier Dynamics

W. G. Harter

Now we consider the transfer operator from Hell, the time evolution operator U. This "grim-reaper" of the quantum world determines everything that happens in a non-relativistic (Schrodinger) system. Nothing escapes U-action including you! So learn U well, and pay particular attention to U's generator H which is called the Hamiltonian. The expression e^{-iHt} (for constant H) is an icon of modern quantum theory. Quantum dot systems from Chapters 7 and 8 will be used as examples and provide our first introduction to quantum periodic band theory and quantum "revival" beats. (Yes, some waves can survive the grim reaper by reviving repeatedly while doing arithmetic, too!)

Chapter 9. Time Evolution and Fourier Dynamics

9.1 Time Evolution Operator

It is often said that nothing that is more demanding than the test of time. All the analyzer experiments considered so far have required time to do, lots and lots of time. Never forget that all our fancy theory of analyzers and wave mechanics is just giving us probabilities; not too different from odds posted at the racetrack. Millions of counts need to be registered before those fancy predictions are seen in a laboratory, and all that counting takes time.

Now we consider a very demanding kind of analyzer, good old Father Time, in the form of *the time evolution operator* $\mathbf{U}(t_{FINAL}, ; t_{INITIAL})$. This "grim reaper" is supposed to be able to take any state at an initial time and transform it into what the state will be at a later time.

$$|\Psi(t_{FINAL},)\rangle = \mathbf{U}(t_{FINAL} ; t_{INITIAL}) \ |\Psi(t_{INITIAL})\rangle \qquad (9.1.1)$$

The main task of this section will be to begin theory and derivation of **U** operators. This is the main problem of quantum theory, so we won't finish the job here. In fact, we won't be done with **U** operators until the twelfth hour of never!

Let's first suppose *time translation symmetry* is present. By that I mean there is no one (such as perfidious janitors) "messing" with our analyzers. So, the experiments run the same day and night. Then we can often simplify the evolution operator equation by just having one time variable as follows

$$|\Psi(t)\rangle = \mathbf{U}(t ; 0) \ |\Psi(0)\rangle \ , \qquad (9.1.2)$$

so you may pick a "time origin" ($t=0$) arbitrarily.

(a) Planck's oscillation hypothesis

At first, the time evolution problem looks formidable, even for a little six-state beam analyzer problem that was studied in Chapter 8. Its evolution equation (9.1.2) looks like the following at any point z in the beam and varies with z. We will put off discussing z-dependence until a later chapter.

$$\begin{pmatrix} \langle 1|\Psi(t)\rangle \\ \langle 2|\Psi(t)\rangle \\ \langle 3|\Psi(t)\rangle \\ \langle 4|\Psi(t)\rangle \\ \langle 5|\Psi(t)\rangle \\ \langle 6|\Psi(t)\rangle \end{pmatrix} = \begin{pmatrix} U_{11} & U_{12} & U_{13} & U_{14} & U_{15} & U_{16} \\ U_{21} & U_{22} & U_{23} & U_{24} & U_{25} & U_{26} \\ U_{31} & U_{32} & U_{33} & U_{34} & U_{35} & U_{36} \\ U_{41} & U_{42} & U_{43} & U_{44} & U_{45} & U_{46} \\ U_{51} & U_{52} & U_{53} & U_{54} & U_{55} & U_{56} \\ U_{61} & U_{62} & U_{63} & U_{64} & U_{65} & U_{66} \end{pmatrix} \bullet \begin{pmatrix} \langle 1|\Psi(0)\rangle \\ \langle 2|\Psi(0)\rangle \\ \langle 3|\Psi(0)\rangle \\ \langle 4|\Psi(0)\rangle \\ \langle 5|\Psi(0)\rangle \\ \langle 6|\Psi(0)\rangle \end{pmatrix} \qquad (9.1.3a)$$

Here the matrix elements are

$$U_{pq} = \langle p|\mathbf{U}(t ; 0)\,|q\rangle \qquad (9.1.3b)$$

How in the world can one derive all those $N^2=36$ time functions U_{pq} ? Woe is us!

But wait! The **U**-operator and any matrix representing it should have the C_N symmetry of the analyzer system shown in Fig. 9.1.1. And, like the analyzer **T**-operator, it should be reduced by the Fourier C_N -symmetry

$|k_m\rangle$ basis to a diagonal matrix made of phase factors $e^{i\phi m}$ as in (9.1.17b). Furthermore, the Planck hypothesis indicates that the phase factors should have the time phasor "clock" form $e^{-i\omega m t}$ that is conventional clockwise phasor rotation. Then the **U**-operator in (9.1.3) can be made to have a much simpler form if the basis is changed to its eigenbasis $|k_m\rangle$ as shown below.

$$\begin{pmatrix} \langle k_0|\Psi(t)\rangle \\ \langle k_1|\Psi(t)\rangle \\ \langle k_2|\Psi(t)\rangle \\ \langle k_3|\Psi(t)\rangle \\ \langle k_4|\Psi(t)\rangle \\ \langle k_5|\Psi(t)\rangle \end{pmatrix} = \begin{pmatrix} e^{-i\omega_0 t} & 0 & 0 & 0 & 0 & 0 \\ 0 & e^{-i\omega_1 t} & 0 & 0 & 0 & 0 \\ 0 & 0 & e^{-i\omega_2 t} & 0 & 0 & 0 \\ 0 & 0 & 0 & e^{-i\omega_3 t} & 0 & 0 \\ 0 & 0 & 0 & 0 & e^{-i\omega_4 t} & 0 \\ 0 & 0 & 0 & 0 & 0 & e^{-i\omega_5 t} \end{pmatrix} \bullet \begin{pmatrix} \langle k_0|\Psi(0)\rangle \\ \langle k_1|\Psi(0)\rangle \\ \langle k_2|\Psi(0)\rangle \\ \langle k_3|\Psi(0)\rangle \\ \langle k_4|\Psi(0)\rangle \\ \langle k_5|\Psi(0)\rangle \end{pmatrix} \quad (9.1.4)$$

Now, instead of $N^2=36$ unknown U_{pq} functions we have only $N=6$ frequency values ω_m to derive.

This is quite a simplification, if true. It is also a reasonable one since the evolution operators need to form a group called the *time evolution group* that multiplies as follows. (Recall (1.4.12d).)

$$\mathbf{U}(t_3\,;t_1) = \mathbf{U}(t_3\,;t_2)\cdot\mathbf{U}(t_2\,;t_1) \quad (9.1.5a)$$

Also, axioms 1-4 require $\mathbf{U}(t_2\,;t_1)$ to be unitary operators. (Recall (1.5.5b).)

$$\mathbf{U}^\dagger(t_2\,;t_1) = \mathbf{U}^{-1}(t_2\,;t_1) = \mathbf{U}(t_1\,;t_2) \quad (9.1.5b)$$

These requirements are satisfied by the Planck phasor forms in the diagonal matrix (9.1.4) or as follows,

$$\mathbf{U}(t_2\,;t_1) = \text{diag}\{\, e^{-i\omega_0(t_2-t_1)}, e^{-i\omega_1(t_2-t_1)}, .. e^{-i\omega_m(t_2-t_1)}, \ldots \,\} \quad (9.1.6a)$$

since

$$e^{-i\omega_m(t_3-t_1)} = e^{-i\omega_m(t_3-t_2)}\, e^{-i\omega_m(t_2-t_1)}, \text{ and } \quad (e^{-i\omega_m(t_2-t_1)})^* = e^{-i\omega_m(t_1-t_2)} \quad (9.1.6b)$$

which depends only on relative time <u>difference</u> $(t_1 - t_2)$: $\mathbf{U}(t_1\,;t_2) = \mathbf{U}(t_1 - t_2\,;0) = \mathbf{U}(0;t_2 - t_1)$

Indeed, we shall demand that a **U**-eigenbasis $\{\, |\omega_0\rangle, |\omega_1\rangle, \ldots |\omega_m\rangle, \,\}$ shall exist even for asymmetric evolution operators for which a convenient symmetry basis $\{\, |k_0\rangle, |k_1\rangle, \ldots |k_m\rangle, \,\}$ is not available to give "instant" diagonalization. We shall describe how to generally find eigenkets $|\omega_m\rangle$ so that

$$\mathbf{U}(t_2\,;t_1)\,|\omega_m\rangle = e^{-i\omega_m(t_2-t_1)}\,|\omega_m\rangle \quad (9.1.7)$$

This is always possible in principle since we know that all unitary operators are diagonalizable. (Recall exercises in Ch. 3.) However, in practice the problem of diagonalization can be a bit of a chore for large systems consisting of millions, billions, or more states! We will need all the help that symmetry analysis can give us.

9.2 Schrodinger Time Equations

Time evolution operators and the states they evolve satisfy time differential equations known as *Schrodinger equations*. This is a common way to restate Planck's oscillation axiom in differential form.

(a) Schrodinger's time equations. Hamiltonian time generators

If time evolution equation (9.1.4) can predict the quantum state future far in advance, then it should certainly give the *rate* of evolution correctly. The time derivative of (9.1.4) is the following.

$$\frac{\partial}{\partial t}\begin{pmatrix} \langle k_0|\Psi(t)\rangle \\ \langle k_1|\Psi(t)\rangle \\ \langle k_2|\Psi(t)\rangle \\ \langle k_3|\Psi(t)\rangle \\ \langle k_4|\Psi(t)\rangle \\ \langle k_5|\Psi(t)\rangle \end{pmatrix} = -i \begin{pmatrix} \omega_0 e^{-i\omega_0 t} & 0 & 0 & 0 & 0 & 0 \\ 0 & \omega_1 e^{-i\omega_1 t} & 0 & 0 & 0 & 0 \\ 0 & 0 & \omega_2 e^{-i\omega_2 t} & 0 & 0 & 0 \\ 0 & 0 & 0 & \omega_3 e^{-i\omega_3 t} & 0 & 0 \\ 0 & 0 & 0 & 0 & \omega_4 e^{-i\omega_4 t} & 0 \\ 0 & 0 & 0 & 0 & 0 & \omega_5 e^{-i\omega_5 t} \end{pmatrix} \bullet \begin{pmatrix} \langle k_0|\Psi(0)\rangle \\ \langle k_1|\Psi(0)\rangle \\ \langle k_2|\Psi(0)\rangle \\ \langle k_3|\Psi(0)\rangle \\ \langle k_4|\Psi(0)\rangle \\ \langle k_5|\Psi(0)\rangle \end{pmatrix}$$

Simplifying the notation and factoring gives (9.2.1)

$$\frac{\partial}{\partial t}\begin{pmatrix} \Psi_{k_0}(t) \\ \Psi_{k_1}(t) \\ \Psi_{k_2}(t) \\ \Psi_{k_3}(t) \\ \Psi_{k_4}(t) \\ \Psi_{k_5}(t) \end{pmatrix} = -i \begin{pmatrix} \omega_0 & 0 & 0 & 0 & 0 & 0 \\ 0 & \omega_1 & 0 & 0 & 0 & 0 \\ 0 & 0 & \omega_2 & 0 & 0 & 0 \\ 0 & 0 & 0 & \omega_3 & 0 & 0 \\ 0 & 0 & 0 & 0 & \omega_4 & 0 \\ 0 & 0 & 0 & 0 & 0 & \omega_5 \end{pmatrix} \bullet \begin{pmatrix} e^{-i\omega_0 t}\Psi_{k_0}(0) \\ e^{-i\omega_1 t}\Psi_{k_1}(0) \\ e^{-i\omega_2 t}\Psi_{k_2}(0) \\ e^{-i\omega_3 t}\Psi_{k_3}(0) \\ e^{-i\omega_4 t}\Psi_{k_4}(0) \\ e^{-i\omega_5 t}\Psi_{k_5}(0) \end{pmatrix} \qquad (9.2.2)$$

Here we lose the Dirac notation briefly with

$$\Psi_{km}(t) = \langle k_m|\Psi(t)\rangle = e^{-i\omega_m t}\langle k_m|\Psi(0)\rangle = e^{-i\omega_m t}\,\Psi_{km}(0)\,. \qquad (9.2.3)$$

Multiplying by $i\hbar$ and then putting back the Dirac notation gives the following.

$$i\hbar\frac{\partial}{\partial t}\begin{pmatrix} \Psi_{k_0}(t) \\ \Psi_{k_1}(t) \\ \Psi_{k_2}(t) \\ \Psi_{k_3}(t) \\ \Psi_{k_4}(t) \\ \Psi_{k_5}(t) \end{pmatrix} = \begin{pmatrix} \hbar\omega_0 & 0 & 0 & 0 & 0 & 0 \\ 0 & \hbar\omega_1 & 0 & 0 & 0 & 0 \\ 0 & 0 & \hbar\omega_2 & 0 & 0 & 0 \\ 0 & 0 & 0 & \hbar\omega_3 & 0 & 0 \\ 0 & 0 & 0 & 0 & \hbar\omega_4 & 0 \\ 0 & 0 & 0 & 0 & 0 & \hbar\omega_5 \end{pmatrix} \bullet \begin{pmatrix} \Psi_{k_0}(t) \\ \Psi_{k_1}(t) \\ \Psi_{k_2}(t) \\ \Psi_{k_3}(t) \\ \Psi_{k_4}(t) \\ \Psi_{k_5}(t) \end{pmatrix}, \qquad (9.2.4a)$$

$$i\hbar\frac{\partial}{\partial t}\begin{pmatrix}\langle k_0|\Psi(t)\rangle\\ \langle k_1|\Psi(t)\rangle\\ \langle k_2|\Psi(t)\rangle\\ \langle k_3|\Psi(t)\rangle\\ \langle k_4|\Psi(t)\rangle\\ \langle k_5|\Psi(t)\rangle\end{pmatrix}=\begin{pmatrix}\hbar\omega_0 & 0 & 0 & 0 & 0 & 0\\ 0 & \hbar\omega_1 & 0 & 0 & 0 & 0\\ 0 & 0 & \hbar\omega_2 & 0 & 0 & 0\\ 0 & 0 & 0 & \hbar\omega_3 & 0 & 0\\ 0 & 0 & 0 & 0 & \hbar\omega_4 & 0\\ 0 & 0 & 0 & 0 & 0 & \hbar\omega_5\end{pmatrix}\bullet\begin{pmatrix}\langle k_0|\Psi(t)\rangle\\ \langle k_1|\Psi(t)\rangle\\ \langle k_2|\Psi(t)\rangle\\ \langle k_3|\Psi(t)\rangle\\ \langle k_4|\Psi(t)\rangle\\ \langle k_5|\Psi(t)\rangle\end{pmatrix}, \tag{9.2.4b}$$

which is called *Schrodinger's time equation*. Its abstract Dirac form is the following

$$i\hbar\frac{\partial}{\partial t}|\Psi(t)\rangle=\mathbf{H}|\Psi(t)\rangle \tag{9.2.5a}$$

where the *Hamiltonian energy operator* **H** is related to $i\hbar$ times the time evolution operator derivative by

$$i\hbar\frac{\partial}{\partial t}\mathbf{U}(t,0)=\mathbf{H}\,\mathbf{U}(t,0) \tag{9.2.5b}$$

and is **H** also called the *generator of time translation*. An exponential solution to (9.1.5b) is

$$\mathbf{U}(t,0)=e^{-i\mathbf{H}t/\hbar}\,\mathbf{U}(0,0)=e^{-i\mathbf{H}t/\hbar}\quad\text{where: }\mathbf{U}(0,0)=\mathbf{1} \tag{9.2.5c}$$

if **H** is an *N-by-N* constant matrix operator as it is in (9.1.4a-b). (It must be constant if there is time translation symmetry. Remember, it is time translation symmetry that permits exponential solutions.)

All of the above "derivations" of Schrodinger's equations (9.2.5) are really only Planck's frequency and energy axiom, starting with (9.1.4) and restated in many fancy ways for an *N*-state system for *N=6*.

(b) Schrodinger's matrix equations

The thing that makes a Hamiltonian **H** powerful is that it may be easily derived it in some other basis like the original channel basis $\{|1\rangle, |2\rangle, ...|N\rangle\}$ and then diagonalized using symmetry techniques or numerical methods to find its eigenvectors $\{|\omega_0\rangle, |\omega_1\rangle, ...|\omega_{N-1}\rangle\}$ known as *energy eigenstates* and eigenvalues $\{\hbar\omega_0, \hbar\omega_1, ...\hbar\omega_{N-1}\}$ known as *energy or frequency spectra* $\varepsilon_m = \hbar\omega_m$. This time, the word *spectra* is used as it was intended by the pioneering spectroscopists who first saw atomic spectral lines in laboratory and in astrophysical observations. (Mathematicians co-opt the term *spectra* other ways.)

Rewriting Schrodinger's time equation (9.2.5a)

$$i\hbar\frac{\partial}{\partial t}|\Psi(t)\rangle=\mathbf{H}|\Psi(t)\rangle \tag{9.2.6a}$$

in an arbitrary basis gives

$$i\hbar\frac{\partial}{\partial t}\begin{pmatrix}\langle 0|\Psi(t)\rangle\\ \langle 1|\Psi(t)\rangle\\ \langle 2|\Psi(t)\rangle\\ \langle 3|\Psi(t)\rangle\\ \langle 4|\Psi(t)\rangle\\ \langle 5|\Psi(t)\rangle\end{pmatrix}=\begin{pmatrix}H_{00} & H_{01} & H_{02} & H_{03} & H_{04} & H_{05}\\ H_{10} & H_{11} & H_{12} & H_{13} & H_{14} & H_{15}\\ H_{20} & H_{21} & H_{22} & H_{23} & H_{24} & H_{25}\\ H_{30} & H_{31} & H_{32} & H_{33} & H_{34} & H_{35}\\ H_{40} & H_{41} & H_{42} & H_{43} & H_{44} & H_{45}\\ H_{50} & H_{51} & H_{52} & H_{53} & H_{54} & H_{55}\end{pmatrix}\bullet\begin{pmatrix}\langle 0|\Psi(t)\rangle\\ \langle 1|\Psi(t)\rangle\\ \langle 2|\Psi(t)\rangle\\ \langle 3|\Psi(t)\rangle\\ \langle 4|\Psi(t)\rangle\\ \langle 5|\Psi(t)\rangle\end{pmatrix}, \tag{9.2.6b}$$

where the matrix elements

$$H_{pq} = \langle p | \mathbf{H} | q \rangle \tag{9.2.6c}$$

are generally non-diagonal except in **H**'s or **U**'s own (eigen) basis $|k_m\rangle$ as in (9.2.4).

(c) Writing Hamiltonian H in terms of symmetry operators $\mathbf{r}^p$

If analyzer **H** -matrix (8.2.1) has C_6 symmetry, it commutes with all the rotation operator **r**-matrices in (2.7.5) and is a linear combination of $\mathbf{r}^p$ as follows.

$$\mathbf{H} = H\,\mathbf{1} + S\,\mathbf{r} + T\,\mathbf{r}^2 + U\,\mathbf{r}^3 + T^*\,\mathbf{r}^4 + S^*\,\mathbf{r}^5, \tag{9.2.6}$$

The $\mathbf{r}^p$-matrices in (2.7.5) combine to give a C_6 -symmetric **H**-matrix Schrodinger equation (9.2.7) in analogy to the **T**-matrix transfer equation (8.2.7), and label its *tunneling paths* from point-to-point.

$$i\hbar\frac{\partial}{\partial t}\begin{pmatrix} \langle 0|\Psi(t)\rangle \\ \langle 1|\Psi(t)\rangle \\ \langle 2|\Psi(t)\rangle \\ \langle 3|\Psi(t)\rangle \\ \langle 4|\Psi(t)\rangle \\ \langle 5|\Psi(t)\rangle \end{pmatrix} = \begin{pmatrix} H & S^* & T^* & U & T & S \\ S & H & S^* & T^* & U & T \\ T & S & H & S^* & T^* & U \\ U & T & S & H & S^* & T^* \\ T^* & U & T & S & H & S^* \\ S^* & T^* & U & T & S & H \end{pmatrix} \bullet \begin{pmatrix} \langle 0|\Psi(t)\rangle \\ \langle 1|\Psi(t)\rangle \\ \langle 2|\Psi(t)\rangle \\ \langle 3|\Psi(t)\rangle \\ \langle 4|\Psi(t)\rangle \\ \langle 5|\Psi(t)\rangle \end{pmatrix}, \tag{9.2.7}$$

The undetermined coefficients *H, S, T, U, T*,* and *S** correspond to all the *tunneling amplitudes* that state $|0\rangle$ could possibly have to other states $|0\rangle$, $|1\rangle$, $|2\rangle$, $|3\rangle$, $|4\rangle$, and $|5\rangle$ as indicated by arrows in Fig. 9.2.1 which are analogous to the transfer amplitude paths for the **T** –matrix (or of a **U**-matrix) in Fig. 8.2.1.

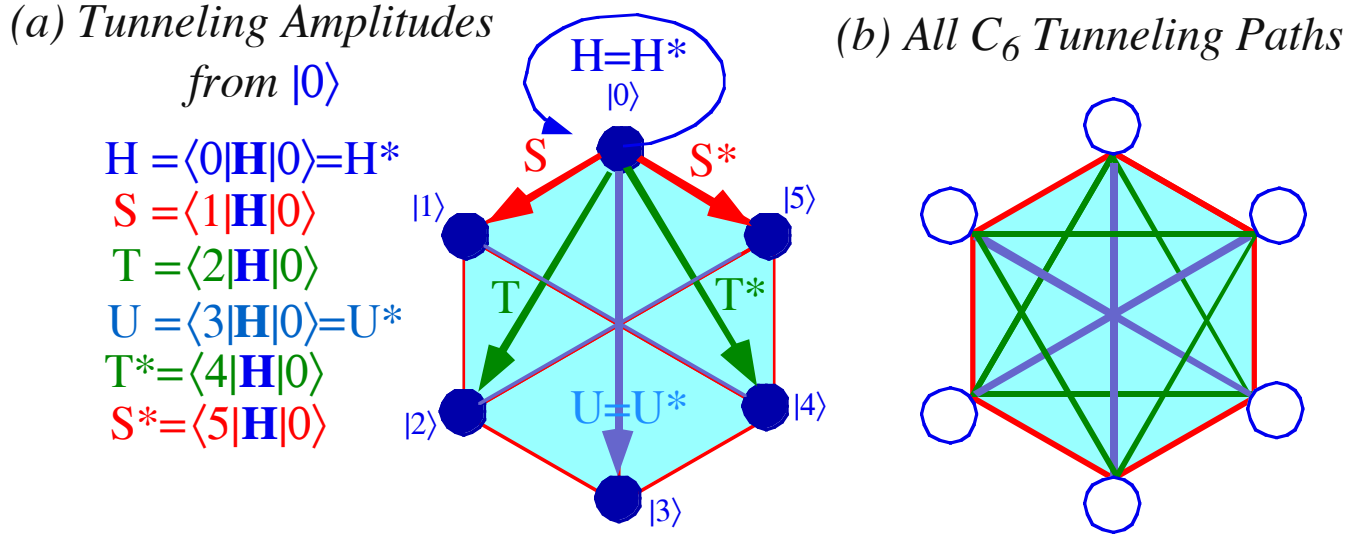

Fig. 9.2.1 Generic 6-channel (C_6)Hamiltonian tunneling (a) Amplitudes (b) Paths

But, there is one important difference. Hamiltonian matrices must be *Hermitian* (self-conjugate: $\mathbf{H}^\dagger = \mathbf{H}$).

$$H_{pq} = \langle p | \mathbf{H} | q \rangle = \langle p | \mathbf{H}^\dagger | q \rangle = H_{qp}{}^* \tag{9.2.8a}$$

Unitary **U** implies Hermitian **H**

Hamiltonian **H** is Hermitian because the time evolution operator is unitary by definition (9.2.5).

$$\mathbf{U}(t,0)^{\dagger} = \left(e^{-i\mathbf{H}t/\hbar}\right)^{\dagger} = e^{i\mathbf{H}^{\dagger}t/\hbar} = \mathbf{U}(t,0)^{-1} = \mathbf{U}(-t,0) = e^{i\mathbf{H}t/\hbar} \tag{9.2.8b}$$

So, an inverse tunneling amplitude such as S^* is the complex conjugate of the forward one S. Also, diagonal components of a Hamiltonian matrix are thus always real.

$$H_{pp} = H_{pp}{}^{*} \tag{9.2.8c}$$

This means the eigenvalues are also real since relations (9.2.8) are true in any basis including the **H** operator's own basis or eigenbasis where **H** is diagonal.

Note that a diametric tunneling amplitude such as $U=U^*$ also is real because its operator $\mathbf{r}^3$ is its own inverse *(*$\mathbf{r}^3 = \mathbf{r}^{3\dagger} = \mathbf{r}^{-3}$*)*. Conjugation reverses direction of rotation for all C_6 operators except **1** and $\mathbf{r}^3$. $\dagger$-conjugation is time reversal for Schrodinger equation (9.2.6). Axiom-2 says bra-clocks run backwards.

9.3 Schrodinger Eigen-Equations

Time evolution is simple for eigenstates $|\omega_m\rangle$ because only a single eigenfrequency ω_m is present. Energy or frequency eigenstates and eigenvalues satisfy *Schrodinger's eigenvalue equation*, also called the *Schrodinger time-independent equation*.

$$\mathbf{H}\,|\omega_m\rangle = \hbar\omega_m\,|\omega_m\rangle = \varepsilon_m\,|\omega_m\rangle \tag{9.3.1a}$$

In a "quantum-dot" basis this is a matrix eigenvalue problem such as the following for $N=6$.

$$\begin{pmatrix} H_{00} & H_{01} & H_{02} & H_{03} & H_{04} & H_{05} \\ H_{10} & H_{11} & H_{12} & H_{13} & H_{14} & H_{15} \\ H_{20} & H_{21} & H_{22} & H_{23} & H_{24} & H_{25} \\ H_{30} & H_{31} & H_{32} & H_{33} & H_{34} & H_{35} \\ H_{40} & H_{41} & H_{42} & H_{43} & H_{44} & H_{45} \\ H_{50} & H_{51} & H_{52} & H_{53} & H_{54} & H_{55} \end{pmatrix} \bullet \begin{pmatrix} \langle 0|\omega_m\rangle \\ \langle 1|\omega_m\rangle \\ \langle 2|\omega_m\rangle \\ \langle 3|\omega_m\rangle \\ \langle 4|\omega_m\rangle \\ \langle 5|\omega_m\rangle \end{pmatrix} = \hbar\omega_m \begin{pmatrix} \langle 0|\omega_m\rangle \\ \langle 1|\omega_m\rangle \\ \langle 2|\omega_m\rangle \\ \langle 3|\omega_m\rangle \\ \langle 4|\omega_m\rangle \\ \langle 5|\omega_m\rangle \end{pmatrix}, \tag{9.3.1b}$$

The Schrodinger time equation (9.2.6b) is a simple 1-dimensional relation for each amplitude.

$$i\hbar\frac{\partial}{\partial t}\langle p|\omega_m\rangle = \langle p|\mathbf{H}|\omega_m\rangle = \hbar\omega_m\langle p|\omega_m\rangle \tag{9.3.2}$$

Its solution has each amplitude $\langle p|\omega_m\rangle$ spinning its clock at the same rate ω_m at constant size $|\langle p|\omega_m\rangle|^2$.

$$\langle p|\omega_m(t)\rangle = \langle p|\omega_m(0)\rangle e^{-i\omega_m t} \tag{9.3.3}$$

$$|\langle p|\omega_m(t)\rangle|^2 = |\langle p|\omega_m(0)\rangle|^2 = const. \tag{9.3.4}$$

Such is the fate of an eigenstate or stationary state. Its observable probability distribution is forever fixed.

But, how does one find just the right $\langle p|\omega_m\rangle$ amplitudes to solve (9.3.1)? Aren't we back in hot water again with $N^2=36$ unknown constants H_{pq} and a big diagonalization job facing us? Woe is us, again! But, fortunately, there are all kinds of techniques and approximation tricks to find the Hamiltonian matrix elements and then find the energy spectrum. That is what most of the rest of the book is about!

Chief among the eigensolution techniques is symmetry analysis. The time evolution matrix **U** and the Hamiltonian matrix **H** for the C_6 -analyzer in Fig. 8.1.1 can be treated to the same techniques that worked for the analyzer **T**-matrix. Again, all possible C_6–symmetric Hamiltonian matrices are given with a single complete set

of eigensolutions. Then all possible motions are obtained from combinations of eigensolutions, which, by their completeness are able to produce an arbitrary initial condition.

After that, the motion is just the interference beating between all the eigenfrequencies that participate in producing a given initial state. Remember, it takes two to tango! At least two eigenstates with different eigenfrequencies need to be up and spinning to have observable motion. Otherwise, nothin's happening!

It turns out that while it takes two to tango, three's a crowd! Two state systems are unique in their harmonic simplicity. At the end of this unit we will see how to understand more complicated *3, 4, 5,...*level excitations for some simple systems.

(a) Solving Schrodinger's eigen-equations for C_6 system

H-eigenvalues use **r**-expansion (9.2.6) of **H** and C_6 symmetry $\mathbf{r}^p$-eigenvalues from (8.2.9).

$$\langle k_m|\mathbf{r}^p|k_m\rangle = e^{-ipk_m a} = e^{-ipm2\pi/N} \quad \text{where:} \quad k_m = m(2\pi/Na)$$

$$\langle k_m|\mathbf{H}|k_m\rangle = H\langle k_m|\mathbf{1}|k_m\rangle + S\langle k_m|\mathbf{r}|k_m\rangle + T\langle k_m|\mathbf{r}^2|k_m\rangle + U\langle k_m|\mathbf{r}^3|k_m\rangle + T^*\langle k_m|\mathbf{r}^4|k_m\rangle + S^*\langle k_m|\mathbf{r}^5|k_m\rangle$$
$$= H + S\,e^{-ik_m a} + T\,e^{-i2k_m a} + U\,e^{-i3k_m a} + T^*\,e^{i2k_m a} + S^*\,e^{ik_m a} \qquad (9.3.5a)$$

Again we check that **H** eigenvectors $|\omega_m\rangle$ are the $|k_m\rangle$ in (8.2.11) which solved transfer matrix **T**.

$$\begin{pmatrix} H & S^* & T^* & U & T & S \\ S & H & S^* & T^* & U & T \\ T & S & H & S^* & T^* & U \\ U & T & S & H & S^* & T^* \\ T^* & U & T & S & H & S^* \\ S^* & T^* & U & T & S & H \end{pmatrix} \bullet \begin{pmatrix} 1 \\ e^{ik_m a} \\ e^{i2k_m a} \\ e^{i3k_m a} \\ e^{-i2k_m a} \\ e^{-ik_m a} \end{pmatrix} = \hbar\omega_m \begin{pmatrix} 1 \\ e^{ik_m a} \\ e^{i2k_m a} \\ e^{i3k_m a} \\ e^{-i2k_m a} \\ e^{-ik_m a} \end{pmatrix} \qquad (9.3.5b)$$

Because of Hermiticity ($\mathbf{H}^\dagger = \mathbf{H}$) eigenvalues ω_m or ε_m will be real eigenfrequency and energy spectra.

$$\hbar\omega_m = \varepsilon_m = H + S\,e^{-ik_m a} + T\,e^{-i2k_m a} + U\,e^{-i3k_m a} + T^*\,e^{i2k_m a} + S^*\,e^{ik_m a} \qquad (9.3.5c)$$

$$\hbar\omega_m = \varepsilon_m = H + 2|S|\,cos(\,k_m a - \sigma\,) + 2|T|\,cos(\,2k_m a - \tau\,) - U\,(-1)^m \qquad (9.3.5d)$$

Here we note: $e^{-i3k_m a} = e^{-i3\pi m} = (-1)^m$ for $N=6$. Also, let the complex parameters be in polar form.

$$S = |S|\,e^{i\sigma}\,, \qquad T = |T|\,e^{i\tau} \qquad (9.3.5e)$$

Their phase angles σ and τ correspond to what is sometimes called a *gauge symmetry breaking* or *Zeeman splitting* parameters. To begin the discussion, we shall let the phase angles be zero or pi.

A little physical intuition helps to make some sense of the energy eigenvalues. The parameters *S*, *T*, and *U* are called *tunneling amplitudes* because they are "sneak factors" that tell how rapidly (and with what phase σ, $\tilde{\tau}$) an evanescent wave in one channel can sneak or tunnel over to one of its neighbors as indicated in Fig. 9.2.1. The *S, T, U* give *rates* at which the *A, B, C* amplitudes of a **T** or **U** matrix grow.

(b) Energy spectrum and tunneling rates

We saw how the evanescent waves in (6.3.10a) of Sec. 6.3c(3) decay exponentially and die off with distance. Channel waves are like this, a channel wave state $|0\rangle$ will be exponentially more likely to tunnel to its nearest neighbor channels $|1\rangle$ or $|5\rangle$ than to more distant channels $|2\rangle$, $|3\rangle$, or $|4\rangle$ in Fig. 9.2.1. So, the distant tunneling amplitudes *U* and *T* might be approximated by zero in (9.3.5d) to give

$$\hbar\omega_m = \varepsilon_m = H + 2|S|\,cos(\,k_m a - \sigma\,)\,. \qquad (9.3.5f)$$

This is an elementary *Bloch dispersion relation*. If wavevector k_m were a continuous variable *k* the dispersion function $\omega(k)$ would trace a cosine as shown in Fig. 9.3.1 where the gauge phase is set to pi ($\sigma=\pi$) to make the k_0 state lowest. Now the spectra correspond to hexagonal projections of $e^{i2\pi m/6}$.

$$\hbar\omega_m = \varepsilon_m = H - 2|S|\,cos(\,k_m a\,)\,. \qquad (\sigma=\pi\,) \qquad (9.3.5g)$$

Note that while the eigenvalues ($\hbar\omega_m = \varepsilon_m$) vary with parameters *H, S, T*, or *U*, the eigen*vectors* $|\omega_m\rangle$ or eigen*functions* $\psi_m(x_p)$ are the same for all values of parameters due to C_N -symmetry.

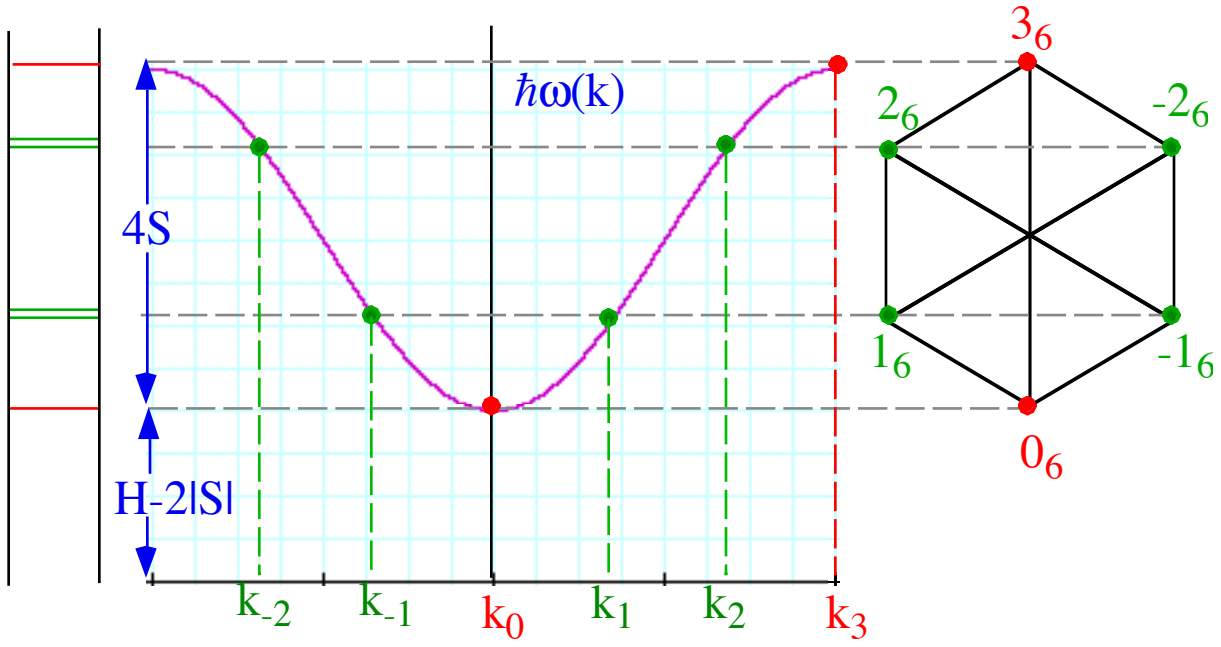

Fig. 9.3.1 Generic 6-channel (C_6) tunneling spectra and Bloch dispersion.

If the tunneling phase σ increases by π/12 it shifts the dispersion relation to the right by π/12 in k-space. It rotates the hexagonal spectral diagram by π/12 or *15°* as shown in Fig. 9.3.2. The resulting spectra shifts and splits the degenerate doublets $\pm 1_6$ and $\pm 2_6$.

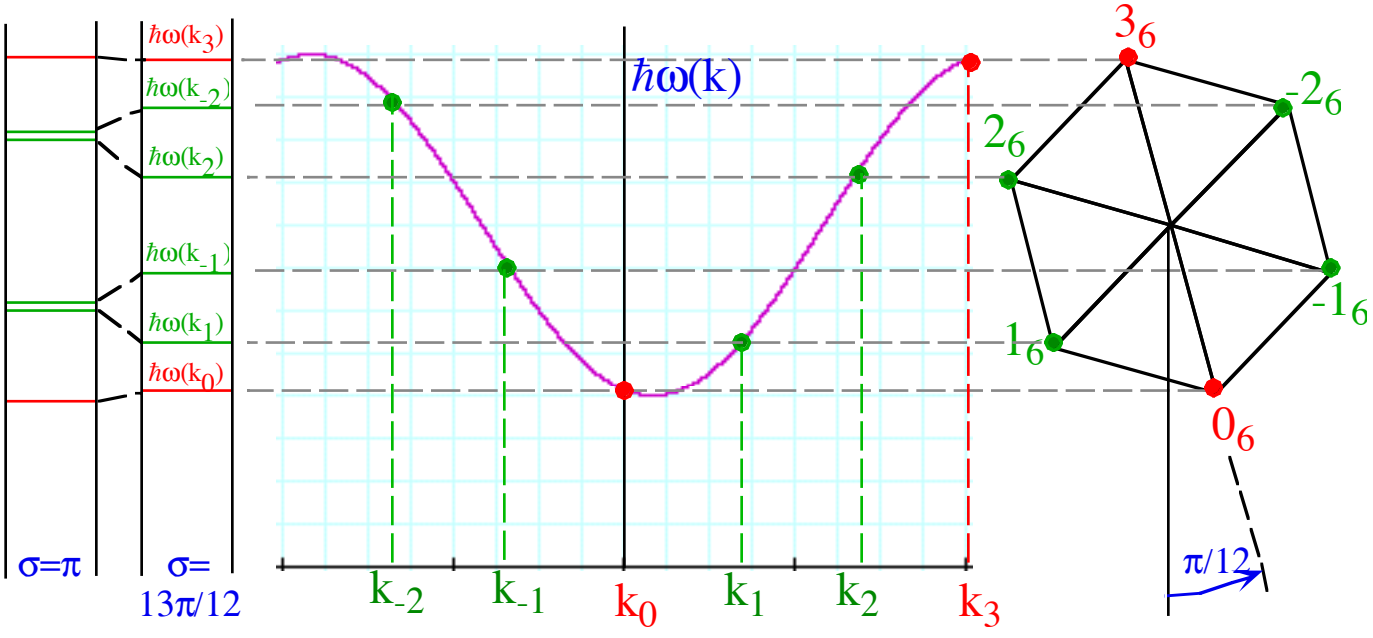

Fig.9.3.2 Same 6-channel (C_6) tunneling spectra with broken symmetry and doublet splitting

This is equivalent to rotating the analyzer disk in Fig. 8.1.1 at a constant negative or clockwise velocity so negatively moving waves increase in energy while the positively moving ones have less energy.

Such a tunneling phase or gauge factor causes a *right-left symmetry breaking* so right-handed and left-handed waves are no longer degenerate in energy. It is analogous to the Doppler shift that is observed by an observer moving through a monochromatic standing wave and sees red-shifted and blue-shifted frequencies while the stationary observer sees equal frequencies. (Recall Sec. 4.2.)

A similar effect occurs if a magnetic field is applied perpendicular to the plane of the analyzer along a beam of charged particles. Then the splitting of doublets is called *Zeeman splitting* which is a very well known atomic spectral effect that will be studied later.

Bloch's waves vs. Bohr's

One should compare the discrete Bloch spectra and dispersion in Fig. 9.3.1 here to the simple Bohr spectra in Fig. 7.1.1. The orbital wavefunctions for both have a plane-wave form of "Bohr's ghost" waves.

$$\psi_m(x) = e^{ik_m x} \qquad (9.3.6a)$$

However, Bloch waves for C_6 are discretized into $N=6$ phasors at discrete points x_p. ($p=1, 2, ...,6$)

$$\psi_m(x_p) = e^{ik_m x_p} = e^{i2\pi mp/N} \qquad (9.3.6b)$$

Each Bloch quantum number $m=0, 1, 2, ..., 5$, is a number *m-modulo-6* as in (7.3.7) and in Fig. 7.3.3.

Bloch eigenvalues, however, differ from Bohr's. Bohr orbital dispersion or energy is a simple parabola (7.1.16) as follows using momentum quantization $p_m=\hbar k_m=\hbar 2\pi m/L$ with: $m=0, \pm1, \pm2,\ldots$

$$E_m = (\hbar k_m)^2/2M = m^2\,[h^2/2ML^2] \qquad (9.3.7)$$

This parabola is a low-energy approximation to the relativistic hyperbola in Fig. 5.2.1. In contrast, the Bloch curve is a flipped cosine function (9.3.5g) as plotted in Fig.9.3.3 and superimposed upon the Bohr parabola. For larger N (Fig. 9.3.3 it is $N=24$) and small m the cosine curve is approximated by a Bloch-like parabola given by a Taylor expansion at the origin ($k=0=k_0$) in k-space.

$$\hbar\omega_m = E_m = H - 2|S|\cos(k_m a) = H - 2|S| + |S|(k_m a)^2 + .. \qquad (9.3.8)$$

In this limit the Bloch dispersion is approximated by the simple Bohr parabola.

In the limit of large number N of "quantum dot" coordinates x_p. ($p=1, 2, 3, 4, ...,N$) the continuum coordinate x of the Bohr orbitals is approached. As long as the waves considered have low k_m , that is, are long compared to the lattice interval $a=L/N$ that divides up the Bohr coordinate range L, then Bohr and Bloch waves have nearly the same dispersion $\omega_m(k_m)$ and will behave the same.

(c) Brillouin's boundary

For larger wavevector k_m the wavelength becomes shorter until its waves begin to "fall through the cracks" in the lattice. Recall the difficulty in following the "Bohr's ghost" wave through the C_6 phasors in Fig. 7.3.3 for the higher waves $(m)_N = (4)_6$ or $(5)_6$, or even $(2)_6$. A break occurs when a half-wave length matches the lattice spacing a. This is when $(m)_N = (N/2)_N = (3)_6$, a "half-way point" known as the *first Brillouin zone boundary (BZB-1)*. It is at k_{12} or $(m)_N = (12)_{24}$ in Fig. 9.3.3 ($N=24$).

$$(m)_{BZB\text{-}1} = (N/2) \text{ or: } k_{BZB\text{-}1} = \pi/a \text{ or: } \lambda_{BZB\text{-}1} = 2a \qquad (9.3.9a)$$

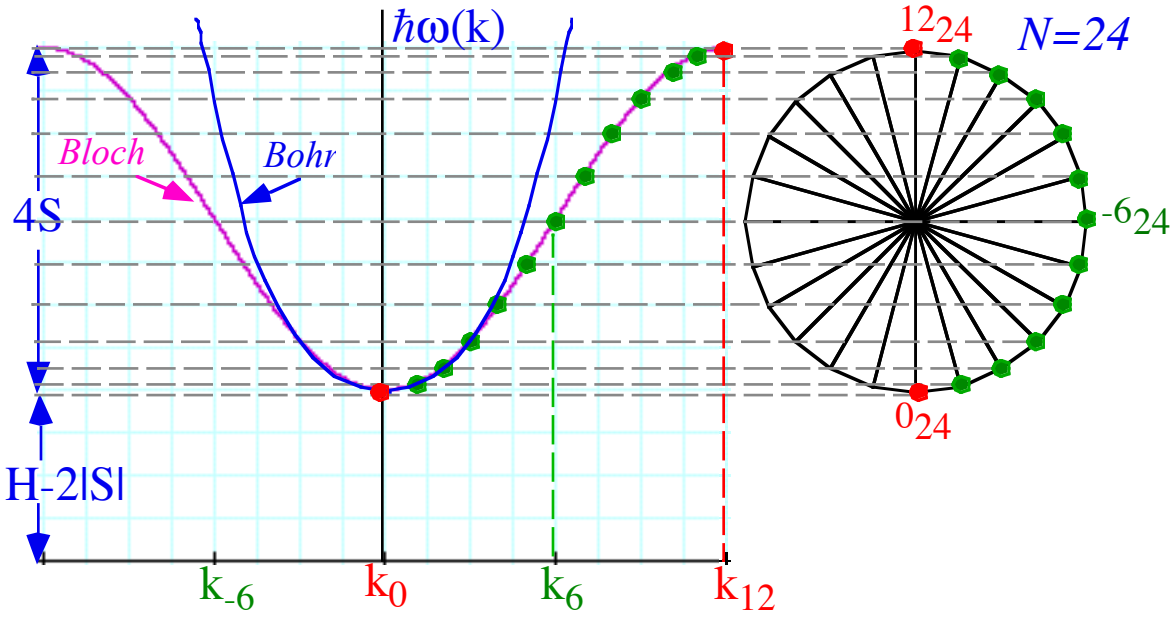

Fig.9.3.3 Generic 24-channel (C_{24}) tunneling spectra and Bohr vs. Bloch dispersion.

At this *m*-number or *k*-value the wave amplitudes are alternating ±*1* at the lattice points x_p.

$$\psi_{N/2}(x_p) = e^{ik_{N/2}x_p} = e^{i2\pi(N/2)p/N} = e^{i\pi p} = (-1)^p \qquad (9.3.9b)$$

Phases that are in or π-out of phase make a standing wave with zero group velocity as in Fig. 9.3.4.

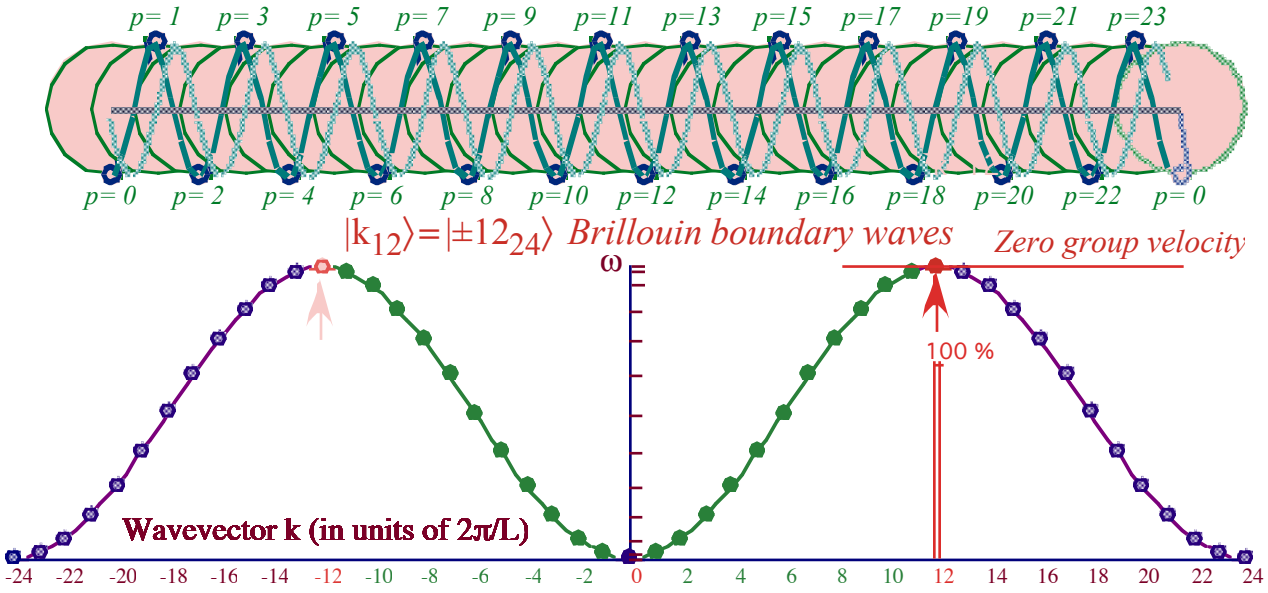

Fig.9.3.4 (C_{24}) Brillouin boundary wave must be standing. (No group velocity)

Postive or negative (*k*=±*12*) waves have the same effect on the 24 lattice points; both give standing wave motion with no transmission one way or the other. In C_{24} symmetry *+12 mod 24 = -12 mod 24*.

The wave group velocity is the velocity V_{group} associated with classical particle or "message" velocity. (Recall discussions in Sec. 4.4 (b-c).) From (9.3.8) the V_{group} for Bloch (or for low-*k* Bohr) is

$$V_{group} = \frac{d\omega_m}{dk_m} = 2\frac{|S|}{\hbar} a \sin(k_m a) \quad \left(\cong 2\frac{|S|}{\hbar} k_m a^2 \text{ , for: } k_m << \pi / a \right) \qquad (9.3.10)$$

The group velocity goes to zero at the origin (k_m=0) and at the Brillouin zone boundary (k_m=k_{BZB}). This is consistent with our picture Fig. 9.3.4 of a standing wave. It just goes nowhere but up and down.

Effective mass: Another quantum view of inertia

Low velocity *(u<<c)* particle momentum is mass times particle velocity: $Mu=MV_{group}$. DeBroglie relation (5.2.5c) gives momentum as $\hbar k_m$. For low-k_m-Bloch waves (Bohr waves), (9.3.10) gives V_{group} proportional to the tunneling amplitude S implying an *effective mass* M_{eff} inversely proportional to S.

$$M_{eff}(0) = \hbar^2/(\,2|S|\,a^2\,) \qquad (9.3.11a)$$

This is consistent with a comparison of Bohr energy values $\varepsilon_m = {}^1/_2(\hbar k_m)^2/_M$ and the low-k_m Bloch energy eigenvalues (9.3.8). Recall the quantum effective mass introduced in (5.3.13) and repeated here.

$$M_{eff} = \frac{F}{a} = \frac{\hbar\dot{k}}{\left(\frac{dV_{group}}{dt}\right)} = \frac{\hbar\dot{k}}{\left(\frac{dV_{group}}{dk}\frac{dk}{dt}\right)} = \frac{\hbar}{\left(\frac{d^2\omega}{dk^2}\right)} \quad \text{where: } V_{group} = \frac{d\omega}{dk} \qquad (9.3.11b)$$

Effective mass is inversely proportional to the curvature of the dispersion relation. As k_m increases in Fig. 9.3.3 the effective mass starts out at *k=0* with the $M_{eff}(0)$ value (9.3.11a). Then it increases until it goes to infinity at $k_m = k_{N/4} = k_6$. Then it comes back from negative infinity losing much of its negativity to end up at ($M_{eff}(k_{12})$=-$M_{eff}(0)$) on the Brillouin zone boundary $k_m = k_{N/2} = k_{12}$. There $\omega_{Bloch}(k)$ is a downward curving dispersion like Dirac negative-energy anti-particle band in the lower half of Fig. 5.4.1. But, $\omega_{Bloch}(k)$ in Fig. 9.3.3 differs from a continuum relativistic dispersion relation (5.2.8)

$$E = \hbar\omega_{relativistic} = \pm\sqrt{\left(Mc^2\right)^2 + \left(c\hbar k\right)^2} \qquad (5.2.8)_{repeated}$$

For $\omega_{rela.}(k)$ effective mass approaches infinity only as the momentum or k becomes large. For a vacuum , a constant applied electric field would cause k to increase uniformly. But, for a C_N lattice k-space is periodic so a field causes a charged particle to just oscillate back and forth each time k passes through another Brillouin zone. Based on this, relativistic symmetry appears quite different from that of a Bloch lattice. But then, have we really looked closely enough at that vacuum continuum? It may take some pretty high k-values to do so!

The final sections of this unit are devoted to dynamics of Bohr waves shown in space-time plots of the following Fig. 9.3.5-6. Recall also Fig. 5.5.5-6. The interference anti-nodes that spring up and then vanish are called *revivals*, a term coined by Joe Eberly to describe atom-laser simulations he noticed around 1976. Much of the intricate structure are called *fractional revivals* first noticed in molecular rotor simulations around 1980. Much of the first analyses of fractional revivals, done during the 1990's, involves particle-in-a-box and atomic Rydberg states. However, Bohr orbitals provide the clearest understanding of revivals because of their underlying C_N symmetry.

(Next pages: Figs. 9.3.5a-c)

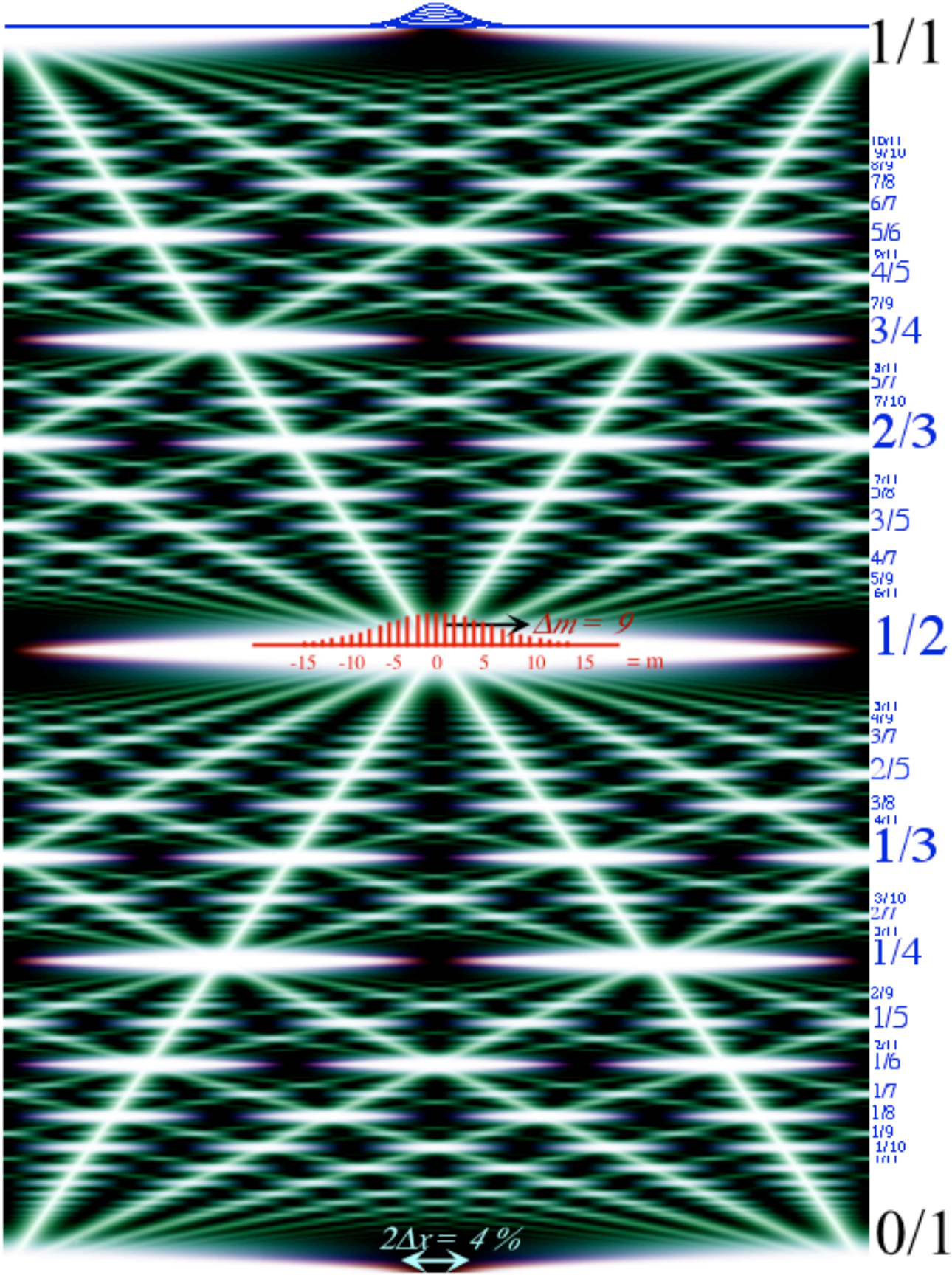
1/1
10/11
9/10
8/9
7/8
6/7
5/6
9/11
4/5
7/9
3/4
8/11
5/7
7/10
2/3
7/11
5/8
3/5
4/7
5/9
6/11
1/2
8/11
4/9
3/7
2/5
3/8
4/11
1/3
3/10
2/7
3/11
1/4
2/9
1/5
2/11
1/6
1/7
1/8
1/9
1/10
1/11
0/1
Δm = 9
-15 -10 -5 0 5 10 15 = m
2Δr = 4 %

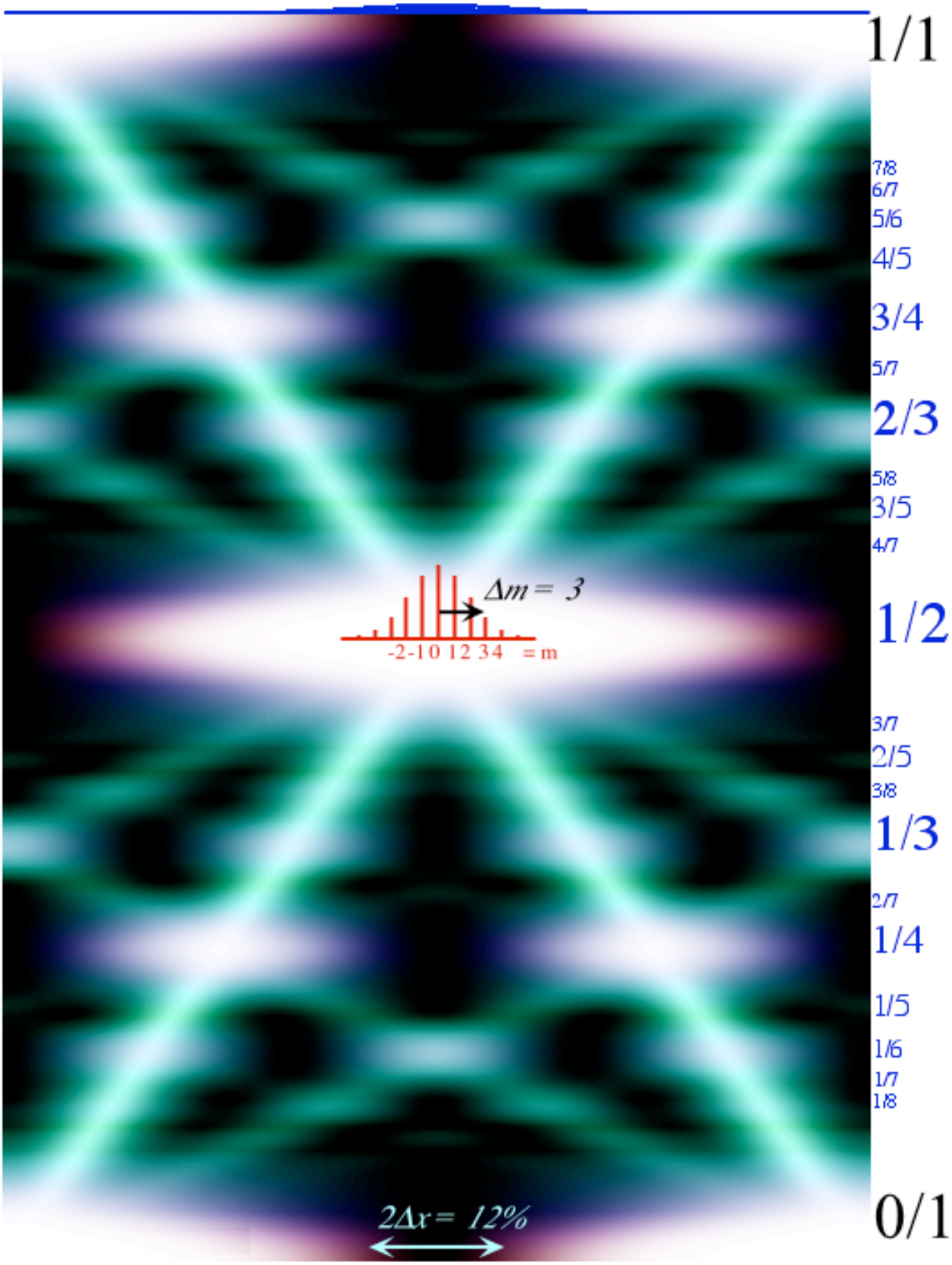
1/1
7/8
6/7
5/6
4/5
3/4
5/7
2/3
5/8
3/5
4/7
1/2
3/7
2/5
3/8
1/3
2/7
1/4
1/5
1/6
1/7
1/8
0/1
Δm = 3
-2-1 0 1 2 3 4 = m
2Δx = 12%

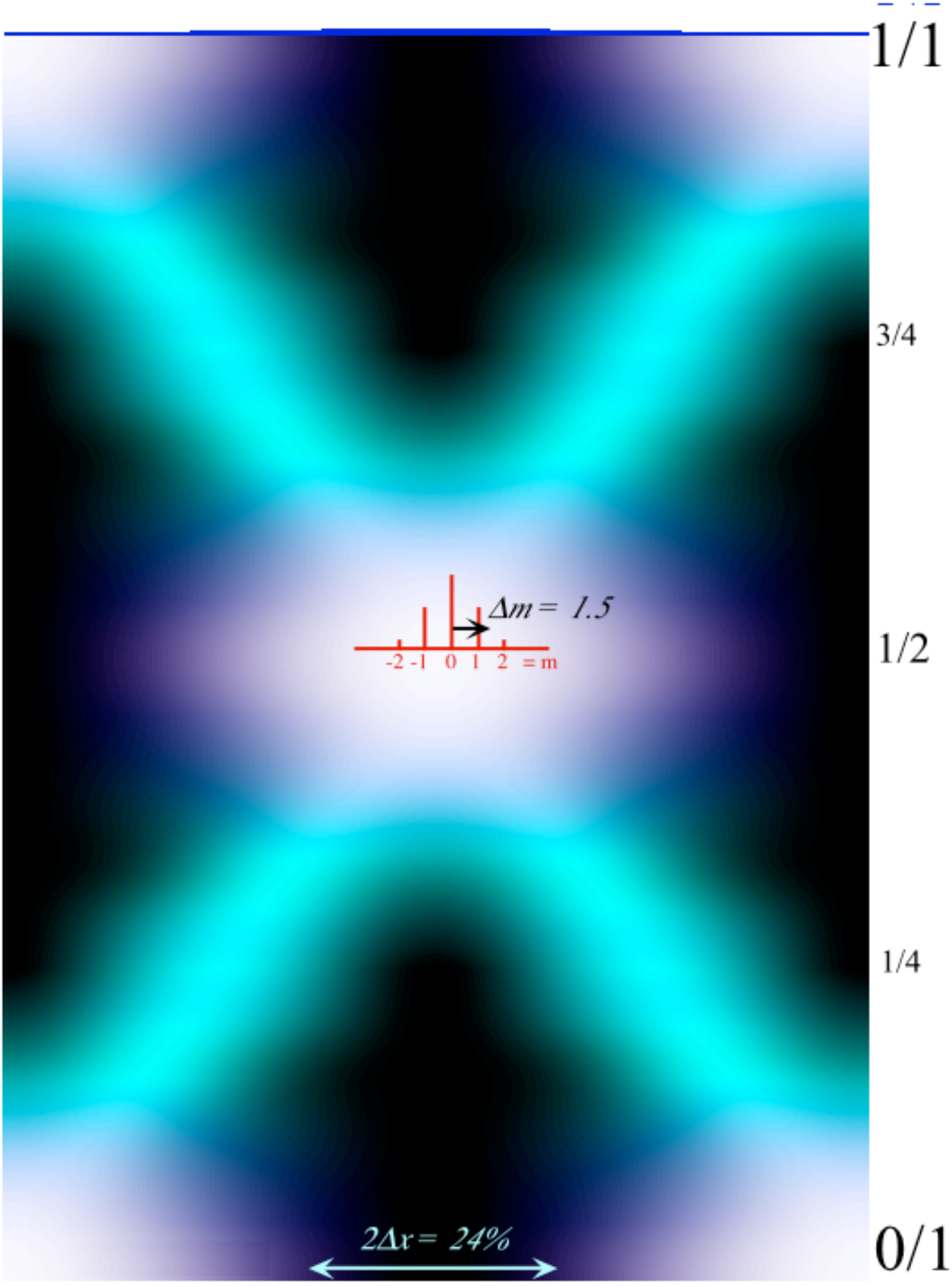

(Preceding pages: Figs. 9.3.5a-c Bohr wavepact revivals in space-time)

(d) Bohr wavepacket dynamics: Uncertainty and revival

We now study Bohr waves that are a Gaussian combination of momentum-m plane waves.

$$\Psi(\phi,0)=\langle\phi,0|\Psi\rangle=\frac{1}{2\pi}\sum_{m=-\infty}^{\infty}e^{-m^2/\Delta m^2}e^{im\phi} \qquad (9.3.12a)$$

Here, $m=0, \pm1, \pm2, \pm3,...$are momentum quantum numbers in Bohr energy formula (9.3.7).

$$E_m=(\hbar k_m)^2/2M=m^2\,[h^2/2ML^2]=m^2h\upsilon_1=m^2\hbar\omega_1 \qquad (9.3.12b))$$

The *fundamental Bohr frequency* $\omega_1=2\pi\upsilon_1$ is the lowest *transition (beat) frequency* $\upsilon_1=(E_1-E_0)/h$. Completing the square of the exponent provides a simpler ϕ-angle wavefunction.

$$\Psi(\phi,0)=\frac{1}{2\pi}\sum_{m=-\infty}^{\infty}e^{-\left(\frac{m}{\Delta m}-i\frac{\Delta m}{2}\phi\right)^2-\left(\frac{\Delta m}{2}\phi\right)^2}=\frac{A(\Delta m,\phi)}{2\pi}e^{-\left(\frac{\Delta m}{2}\phi\right)^2} \qquad (9.3.13a)$$

Only the lower-m terms with $m<\Delta m$ in the sum $A(\Delta m,\phi)$ have significant $e^{-(m/\Delta m)^2}$ values, but for larger Δm the number of significant terms grows until sum A approaches a Gaussian integral independent of ϕ .

$$A(\Delta m,\phi)=\sum_{m=-\infty}^{\infty}e^{-\left(\frac{m}{\Delta m}-i\frac{\Delta m}{2}\phi\right)^2}\xrightarrow[\Delta m>>1]{}\int_{-\infty}^{\infty}dk\,e^{-\left(\frac{k}{\Delta m}\right)^2}=\sqrt{\pi}\Delta m \qquad (9.3.13b)$$

The variable factor $e^{-(\Delta m\,\phi/2)^2}$ is a Gaussian function of angle ϕ or position x. It is remarkable that the Fourier transform of a Gaussian $e^{-(m/\Delta m)^2}$ momentum distribution is a Gaussian $e^{-(\phi/\Delta\phi)^2}$ in coordinate ϕ.

$$\langle m|\Psi\rangle=e^{-(m/\Delta m)^2}\quad\text{implies:}\qquad\langle\phi\,|\Psi\rangle=e^{-(\phi/\Delta\phi)^2} \qquad (9.3.14)$$

The relation between *momentum uncertainty* Δm and *coordinate uncertainty* $\Delta\phi$ is a *Heisenberg relation*.

$$\Delta m/2=1/\Delta\phi\ ,\text{or:}\qquad\Delta m\,\Delta\phi=2 \qquad (9.3.15)$$

A Gaussian is an eigenvector of the Fourier C_n transformation matrix. (More about this later.)

Three space-time plots are given in Fig. 9.3.5a, b, and c, respectively, with decreasing momentum half-width $\Delta m=9,\ 3,$ and 1.5 and courser spatial resolution $\Delta\phi/2\pi=2\%,\ 6\%,$ and 12% . Each is plotted for a full time period $\tau_1=1/\upsilon_1=2\pi/\omega_1$ after which it repeats. The first Fig. 9.3.5a uses fine spatial resolution $\Delta x\cdot=0.02$ which requires 9-quantum excitation $(\Delta m=9)$. It shows a labyrinth of increasingly fine self-similar X-patterns of wave *revivals*. In the second and third figures (9.3.5b and c), of lower excitation ($\Delta m=3,$ and 1.5, respectively), the finer X-patterns begin to disappear leaving one big X over Fig. 9.3.5c.

Semi-classical Theory: Farey Sums and Quantum Speed Limits

Fig. 9.3.5c provides a clue to the theory of revivals. Its X is like a zero crossing in the Lorentz grid in Fig. 4.2.9, but with momentum values restricted by $\Delta m=1.5$ to the first two levels $m=0$, ±1, leaving two group (or phase) velocities $V_{\pm1}=\pm L/\tau_1$ by (4.2.20), that is, a Bohr length L per Bohr time unit τ_1.

$$V_{group}^{Bohr}(m\leftrightarrow n)=\frac{\omega_m-\omega_n}{k_m-k_n}=\frac{(m^2-n^2)h\upsilon_1}{(m-n)h/L}=(m+n)\frac{L}{\tau_1}=(m+n)V_1 \qquad (9.3.16)$$

The X in Fig. 9.3.5c has two zeros doing one lap in opposite directions around the Bohr ring in a Bohr period τ_1. The packet anti-nodes or "particles" do laps, too, but their paths are not as contiguous.

Fig. 4

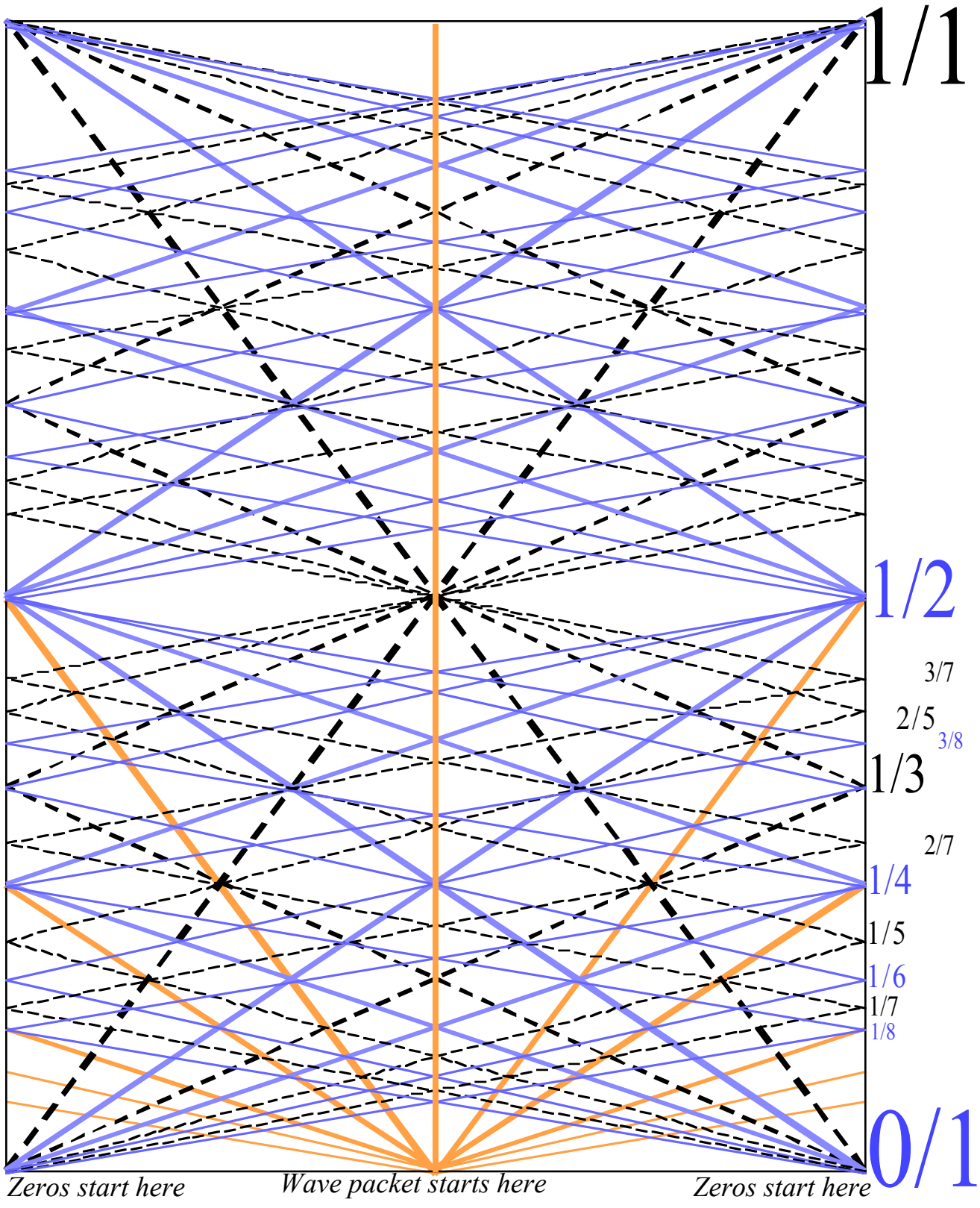

Fig. 9.3.6 Intersecting wave space-time X-path trajectories of nodes and anti-nodes.

(Anti-nodal revival peaks and phases are discussed later.) |Ψ|-nodes, being virtually dead, have an indestructibility not had by zeros of *Re*Ψ that annihilate and re-create as they gallop through Fig. 4.2.9.

Relaxing the momentum uncertainty Δ*m* allows more *m*-values and wave velocities: $\pm V_1, \pm 2V_1, \pm 3V_1, \ldots$ ranging up to $2\Delta m V_1$. By (9.3.16) the maximum lap rate or *quantum speed limit* is 2Δ*m*, *i.e.*, twice the maximum |*m*|. Each velocity gives a fractional lap time of *1/1, 1/2, 1/3, ..., 1/(2Δm)* of the Bohr period. Such fractions are written in the margin of Fig. 9.3.5 at the point where a lap trajectory passes the point $\phi = \pm\pi$ opposite the origin $\phi = 0$ of the wave packet. An *n-th* multiple *n/D* of an allowed fraction *1/D* corresponds to the *n-th* lap of a wave node ("zero") if *D* is odd or the *n-th* lap of a wave anti-node ("particle") if *D* is even.

The *n/D* fractional lines in Fig. 9.3.6 highlight the wave paths in Fig. 9.3.5a. As excitation Δ*m* increases, even-*D* "particle" paths show up as dark shadows in between the odd-*D* "zero" paths in Fig. 9.3.5a. Also seen in a high-Δ*m* plot (Fig. 9.3.5a) are "particle" paths with odd *and* even fractional slopes emanating from the origin $\phi = 0$ of the wave packet. This is indicated in Fig. 9.3.6, too.

The geometry of generic group velocity rays is sketched in Fig. 9.3.7 using two rays to form an asymmetric X around an intersection. (A symmetric X has equal group speeds d_1 and d_2.) Fig. 9.3.5a is a patchwork of self-similar X patterns of nodal *(odd-d_k)* or anti-nodal *(even-d_k)* rays. The equations for the two lines in Fig. 9.3.6 are

$$\phi = -d_1 t + n_1 + 1/2 \qquad \phi = d_2 t - n_2 + 1/2 \qquad (9.3.17)$$

Subtracting the first ϕ equation from the second gives the intersection time for the center of the X.

$$t_{12-intersection} = \frac{n_2 + n_1}{d_2 + d_1} = \frac{n_2}{d_2} \oplus_F \frac{n_1}{d_1} \qquad (9.3.18)$$

The resulting combination is called a *Farey Sum* $\oplus_F$ of the rational fractions n_1/d_1 and n_2/d_2 after John Farey, an 1800's geologist.

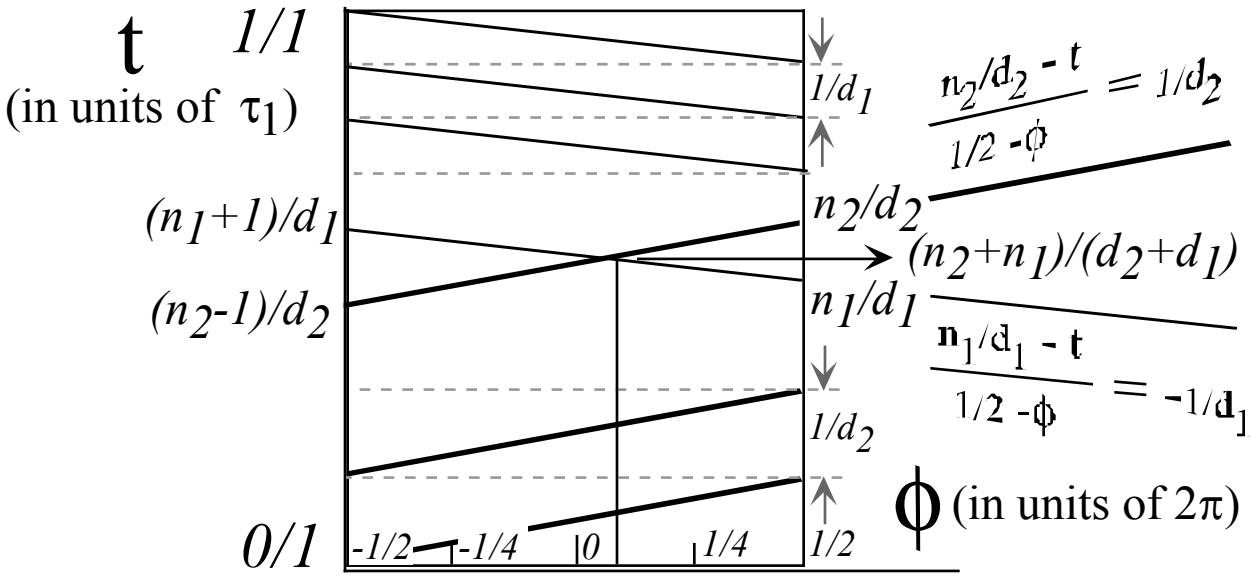

Fig. 9.3.7 Farey-sum geometry and algebra of intersecting wave space-time trajectories.

The Farey sum has been used to analyze classically "chaotic" or "fractal" structures , but its use in organizing quantum resonance structure is new. It begins with a fundamental Farey sum relating the beginning fraction *(0/1)* and ending fraction *(1/1)* of the *(0↔1)*-quantum beat or fundamental revival.

$$\frac{0}{1}\oplus_F\frac{1}{1}=\frac{1}{2} \tag{9.3.19}$$

This is the instant $t/\tau_1=1/2$ for a half-time revival and the zero at the center of the fundamental X in Fig. 9.3.5c. The fundamental sum makes up the second row of a *Farey Tree* of such sums shown in (9.3.20). The sums in the *D-th* row of a Farey tree are an ordered set of all reduced fractions with denominator equal to *D or less*. The tree need not go beyond $D>2\Delta m$ where denominator D exceeds the wave quantum speed limit $2\Delta m$ of (9.3.16). Finer revivals will be unresolvable. More energy is needed to see finer X's.

$D\le 1$	$\frac{\mathbf{0}}{\mathbf{1}}$																					$\frac{\mathbf{1}}{\mathbf{1}}$
$D\le 2$	$\frac{0}{1}$										$\frac{\mathbf{1}}{\mathbf{2}}$											$\frac{1}{1}$
$D\le 3$	$\frac{0}{1}$						$\frac{\mathbf{1}}{\mathbf{3}}$				$\frac{1}{2}$			$\frac{\mathbf{2}}{\mathbf{3}}$								$\frac{1}{1}$
$D\le 4$	$\frac{0}{1}$				$\frac{\mathbf{1}}{\mathbf{4}}$		$\frac{1}{3}$				$\frac{1}{2}$			$\frac{2}{3}$		$\frac{\mathbf{3}}{\mathbf{4}}$					$\frac{1}{1}$
$D\le 5$	$\frac{0}{1}$			$\frac{\mathbf{1}}{\mathbf{5}}$	$\frac{1}{4}$		$\frac{1}{3}$		$\frac{\mathbf{2}}{\mathbf{5}}$		$\frac{1}{2}$		$\frac{\mathbf{3}}{\mathbf{5}}$	$\frac{2}{3}$		$\frac{3}{4}$	$\frac{\mathbf{4}}{\mathbf{5}}$				$\frac{1}{1}$
$D\le 6$	$\frac{0}{1}$			$\frac{\mathbf{1}}{\mathbf{6}}$	$\frac{1}{5}$	$\frac{1}{4}$		$\frac{1}{3}$		$\frac{2}{5}$		$\frac{1}{2}$		$\frac{3}{5}$		$\frac{2}{3}$		$\frac{3}{4}$	$\frac{4}{5}$	$\frac{\mathbf{5}}{\mathbf{6}}$		$\frac{1}{1}$
$D\le 7$	$\frac{0}{1}$		$\frac{\mathbf{1}}{\mathbf{7}}$	$\frac{1}{6}$	$\frac{1}{5}$	$\frac{1}{4}$	$\frac{\mathbf{2}}{\mathbf{7}}$	$\frac{1}{3}$		$\frac{2}{5}$	$\frac{\mathbf{3}}{\mathbf{7}}$	$\frac{1}{2}$	$\frac{\mathbf{4}}{\mathbf{7}}$	$\frac{3}{5}$		$\frac{2}{3}$	$\frac{\mathbf{5}}{\mathbf{7}}$	$\frac{3}{4}$	$\frac{4}{5}$	$\frac{5}{6}$	$\frac{\mathbf{6}}{\mathbf{7}}$		$\frac{1}{1}$
$D\le 8$	$\frac{0}{1}$	$\frac{\mathbf{1}}{\mathbf{8}}$	$\frac{1}{7}$	$\frac{1}{6}$	$\frac{1}{5}$	$\frac{1}{4}$	$\frac{2}{7}$	$\frac{1}{3}$	$\frac{\mathbf{3}}{\mathbf{8}}$	$\frac{2}{5}$	$\frac{3}{7}$	$\frac{1}{2}$	$\frac{4}{7}$	$\frac{3}{5}$	$\frac{\mathbf{5}}{\mathbf{8}}$	$\frac{2}{3}$	$\frac{5}{7}$	$\frac{3}{4}$	$\frac{4}{5}$	$\frac{5}{6}$	$\frac{6}{7}$	$\frac{\mathbf{7}}{\mathbf{8}}$	$\frac{1}{1}$

(9.3.20)

The tracking of crests or wave peaks yields information about classical particle-like or group-wave motion. It is comforting to see familiar classical paths in what is often bewildering quantum cacophony but, the clearest X-paths in Fig. 9.3.5a are *zeros* emanating from the point $\phi=\pm\pi$ where the particle packet originally was *not*. Quantum wave dynamics differs from classical dynamics is that multiple Fourier components easily interfere much of a wave to death. Most path phases lead to *non*-existence except near (rare) stationary-phase paths that may be familiar classical ones. This is what is responsible for particle localization that allows us to enjoy a Newtonian world and largely conceals its quantum wave nature from us. Where the wave is *not* provides important quantum clues. One recalls Sherlock Holmes' revelation that it is the "dog that did *not* bark" which solved a mystery.

9.4 Homo-cyclic Cn Revivals

Wave phase is key to the C_N dynamics beginning with the "beats" of two-state C_2 system. As we have said, "It takes two to tango." First we review the two-state-system dynamics with analogies to optical polarization from Chapter 1 and coupled pendulum dynamics. (Later chapters will use this analogy.) C_2 holds the first key to analyzing the revivals introduced in the preceding section.

We have also said, "Three's a crowd." The dynamics associated with C_3 systems is discussed after that of C_2 and then that of C_4, C_5, C_6, and C_{15} systems. Each is part of the revival milieu of Fig. 9.3.5.

(a) Two–state C_2 systems: Beats

Motion of anti-nodal revivals for a 2-level excitation such as Fig. 9.3.5c are like beats of coupled pendulums. Fig. 9.4.1a shows *phasor* pictures of 2-cyclic (C_2) eigenstates. Phasor "clocks" are phase-space plots of $Re\Psi$ *vs.* $Im\Psi$ for wavefunction $\Psi(p)$ at each spatial point $p=0,1$. $Re\Psi$ is up, $Im\Psi$ is to the left, and the area $\pi|\Psi|^2$ of the phasor is proportional to probability $|\Psi|^2$ at point p.

Each eigenstate phasor rotates clockwise at its Bohr eigenfrequency $\omega_m = m^2\omega_1$, that is, $\Psi(t)=e^{-i\omega_m t}\Psi(0)$. The C_2 eigenstates are labeled *even* $(0_2)=(+)$ or *odd* $(1_2)=(-)$ as usual.

$$|+\rangle = |0_2\rangle = (|x\rangle + |y\rangle)/\sqrt{2} \qquad (9.4.1a) \qquad |-\rangle = |1_2\rangle = (|x\rangle - |y\rangle)/\sqrt{2} \qquad (9.4.1b)$$

$$\text{Bohr eigenfrequency: } \omega_0 = 0 \qquad (9.4.2a) \qquad \text{Bohr eigenfrequency: } \omega_1 \qquad (9.4.2b)$$

$|m_2\rangle$ eigenfrequencies ω_m are $\omega_0 = 0$ and $\omega_1 = h/(2ML^2)$ by (9.3.12b). States $|m_2\rangle$ are + or – combinations of a local oscillator base state labeled $|x\rangle=|r^0\rangle$ (localized at spatial point $p=0$ or $\phi=0$) and a "flipped" base state $|y\rangle=\mathbf{r}|x\rangle=|r^1\rangle$ (localized at point $p=1$ or $\phi=\pi$). States $|+\rangle$ and $|-\rangle$ are also eigenstates of C_2 "flip" operator $\mathbf{r}$ defined by $\mathbf{r}|x\rangle=|y\rangle$ and $\mathbf{r}|y\rangle=|x\rangle$, that is, $\mathbf{r}|+\rangle=+|+\rangle$, and $\mathbf{r}|-\rangle=-|-\rangle$. State $|+\rangle$ is analogous to $+45°$ polarization which is the "slow" eigenstate. State $|-\rangle$ is analogous to the "fast" $-45°$ optical axis.

An initial *50-50* combination of the $|+\rangle$ and $|-\rangle$ eigenstates briefly recovers the $|x\rangle=|r^0\rangle$ local base

$$|x\rangle = (|+\rangle + |-\rangle)/\sqrt{2} = (|0_2\rangle + |1_2\rangle)/\sqrt{2}, \qquad \textit{(Time t=0)}$$

lying between $|+\rangle$ and $|-\rangle$ in Fig. 9.4.1b. The $|1_2\rangle$-eigenstate is faster than the $|0_2\rangle$-eigenstate (which does not move at all by (9.4.2a)) The $|x\rangle$-state is always a sum of 0_2 and 1_2 phasors. (Left and right 0_2 phasors are at 12 PM in Fig. a while the left 1_2 phasor starts at 12 PM and the right 1_2 phasor at 6 PM.) After 12 PM the 1_2 phasors "tick" but 0_2 phasors are stuck at 12PM. Their sum $|x\rangle$ varies with time.

By *1/4* of beat period τ_1, the fast $|1_2\rangle$ clocks are $90°$ ahead of the stuck $|0_2\rangle$. (Clockwise is $-i$.)

$$|L\rangle = (|+\rangle - i|-\rangle)/\sqrt{2} = (|0_2\rangle - i|1_2\rangle)/\sqrt{2}. \qquad \textit{(Time t=(1/4)}\,\tau_1\textit{)}$$

The left and right hand 1_2 clocks move to 3 PM and 9 PM, respectively, but 0_2 clocks are stuck at 12 PM. On the left: 12 PM plus 3 PM is half-size clock at 2:30 PM. On the right: 12 PM plus 9PM is a half-size clock at 10:30 PM. Note two half-phasors at $-45°$ (2:30 PM) and $+45°$ (10:30 PM) at *1/4*-period. The *1/4* period situation is analogous to optical *1/4*-wave plates that change $|x\rangle$-polarization to left-circular $|L\rangle$.

By $\tau_1/2$ the fast 1_2 -clocks go $180°$ ahead to give the "flipped" local base state of y-polarization.

$$|y\rangle = (|+\rangle - |-\rangle)/\sqrt{2} = (|0_2\rangle - |1_2\rangle)/\sqrt{2} \qquad \textit{(Time t=(1/2)}\,\tau_1\textit{)}$$

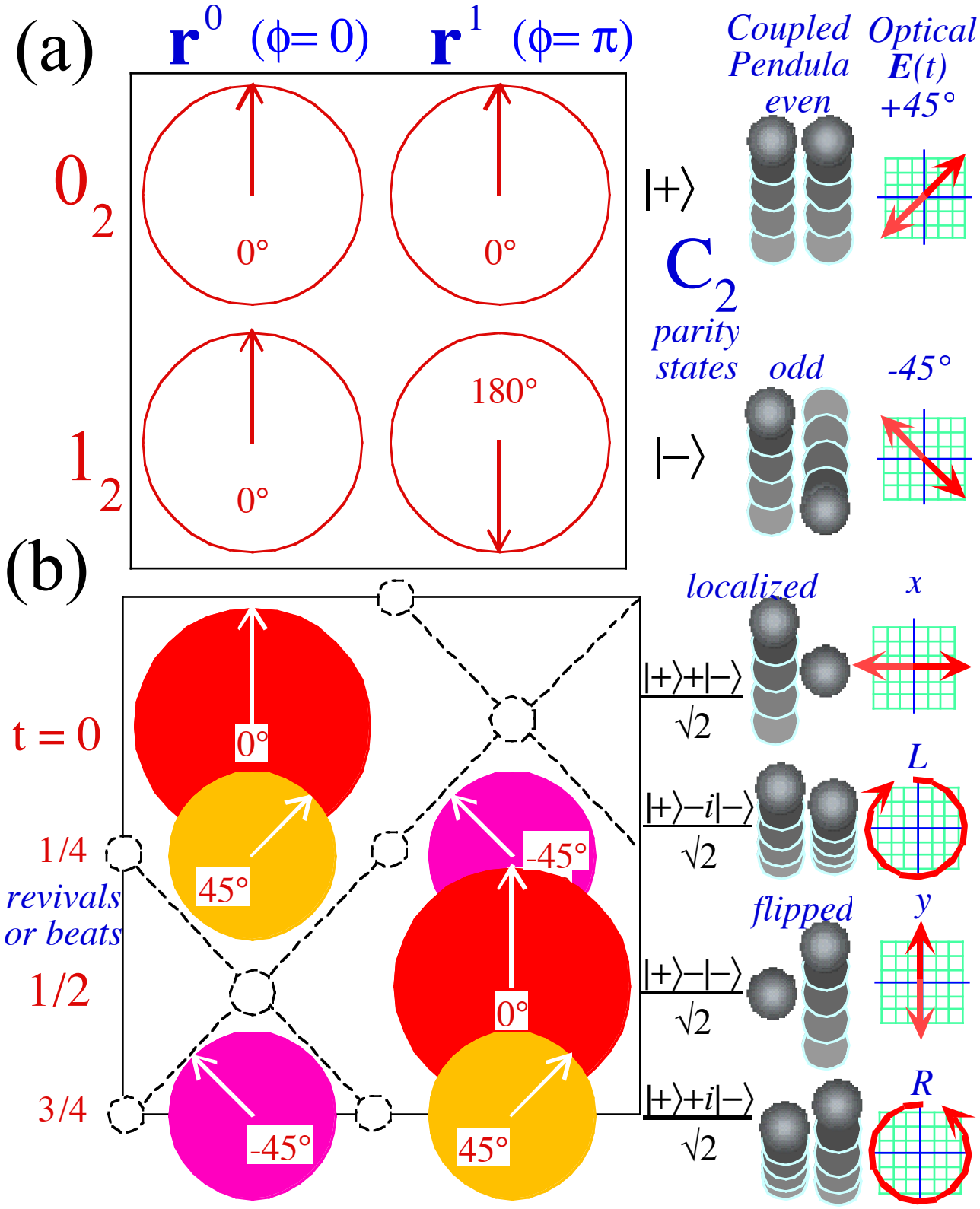

Fig. 9.4.1 (a) C_2 eigenstate phasors. (b) 50% combination states de localizing and reviving.

At $\tau_1/2$, the left 1_2 clock is at 6 PM the right one at 12 PM, but both 0_2 clocks still read 12PM . On the left: 12 PM plus 6 PM is zero (a node). On the right: 12 PM plus 12PM is *big* 12 PM. All the wave flips to the $|y\rangle$-state. The *1/2*-period situation is like *1/2*-wave plate changing $|x\rangle$-polarization to $|y\rangle$.

Still later at $(3\tau_1/4)$ the initial $|x\rangle$-state has become a right circular state. (Fig. 9.4.1b bottom)

$$|R\rangle = (\,|+\rangle + i\,|-\rangle\,)/\sqrt{2} = (\,|0_2\rangle + i\,|1_2\rangle\,)/\sqrt{2} \qquad (Time\ t=(3/4)\,\tau_1\,)$$

Finally, at full-time $(1/1)\tau_1$ the initial $|x\rangle$ state (top of Fig. 9.4.1b) is once again back to being $|x\rangle$ and would reappear beneath Fig. 9.4.1b to begin repeating the revival sequence.

In Fig. 9.4.1b, dotted lines making an X are drawn around the phasors to connect places where wave amplitude is low like the X-pattern in Fig. 9.3.5c. Low *m*-uncertainty $(\Delta m=1.5)$ means the revival wave is mostly a combination of the first two Bohr eigenlevels $m=0$ and $|m|=1$ having just two group (or phase) velocities $+V_1$ and $-V_1$. In other words, Fig. 9.3.5c is essentially just a two-state system, and the major half and full revivals are just binary beat of two coupled symmetric pendulums.

The *1/4* fractional revival corresponds to *transition state* $|L\rangle = (\,|x\rangle - i\,|y\rangle\,)/\sqrt{2}$ (analogous to left circular polarization) between the major revivals. In $|L\rangle$ the left hand position phasor is *90°* ahead of the right hand one being resonantly pumped up. The roles of the two phasors are reversed at $3\tau_1/4$.

(b) C_n group structure: n=3, 4,...6 Eigenstates

To understand finer X-zero patterns and fractional revivals between zeros in Fig. 9.3.5 a-b we go beyond the binary $\{|0_2\rangle|1_2\rangle\}$ basis to, at least, the base-3 basis $\{|0_3\rangle|1_3\rangle|2_3\rangle\}$ of C_3 The bra state vectors $\{\langle 0_3|\langle 1_3|\langle 2_3|\}$ were defined in Fig. 2.6.4 and are re-drawn in Fig. 9.4.2a. The C_3 wave states have quantized momentum *m=0, 1, and 2 modulo 3* . Each *m* labels a row of three phasors in Fig. 9.4.2a which are a discrete sampling of the waves in the first three Bohr levels *m=0,1,* and *2*.

In Fig. 9.4.2b are *4-nary* C_4 base states of *m=0, 1, 2 and 3 modulo 4* quanta and Fig. 9.4.3a reintroduces *5-nary* C_5 bases of *m=0, 1, 2,3, and 4 modulo 5* quanta, and similarly in Fig. 9.4.3b for C_6. These systems are like counters; a binary C_2 system can count only to two, that is, *0* to *1*, but each of the C_N systems are capable of counting to *N*, that is, *0, 1, 2,3,..,N-1*.

Physically the C_N waves are bases of a finite and discrete Fourier analysis. Each C_N *character table* in Fig. 9.4.2a-b or 9.4.3a-b (if all divided by $\sqrt{N}$) is the *N-by-N* unitary *(U(n))* transformation matrix $\langle p|m\rangle$ of *discrete Fourier transformation coefficients*. (Recall Fig. 7.3.3 and discussion.)

$$\left\langle p\middle|(m)_N\right\rangle = e^{i\,p\,m/2\pi N}\ /\sqrt{N} = \left\langle (m)_N\middle|p\right\rangle^* \qquad (p,m = 0,1,2,...,N-1) \qquad (9.4.3a)$$

Each phasor in Fig. 9.4.2-12 sits at one of *N* equally spaced lattice points *p=0, 1, ...,N-1*. Each phasor gives for a particular angular point *p=0, 1, 2,3,..,N-1* the complex wave amplitude (7.3.10a)

$$\psi_{\pm m}(2\pi p/N) = \langle p|(m)_N\rangle = \langle (m)_N|p\rangle^*$$

of a continuous running wave that is one of Bohr-Schrodinger eigenfunctions $\psi_{\pm m}(\phi)$.

A real (cosine) part of the eigenfunction is drawn for each eigenstate $|(m)_N\rangle$ in Fig. 9.4.2-3 to help connect it to the latter. The state notation $(m)_N$ labels these waves and should be read *m-modulo-N* (or *m%N* in *C*) meaning

that waves having $m \pm nN$ wavelengths or quanta will give a physically and mathematically identical state $(m)_N$. (They are Fourier *aliases* $(m)_N = (m \pm nN)_N$, states differing only by reciprocal lattice vectors $K = \pm nN$.)

In Fig. 9.4.2-12 each one of N equally spaced lattice points $p=0, 1, 2, 3,...,N-1$, is labeled by a *p-th* power $\mathbf{r}^p$ of a fundamental C_N group rotation $\mathbf{r}$ by angle $2\pi/N$, that is, by $\mathbf{r}^0=\mathbf{1}$, $\mathbf{r}^1$, $\mathbf{r}^2$, $\mathbf{r}^3$ ... , $\mathbf{r}^{N-1}$, $\mathbf{r}^N=\mathbf{1}$ respectively. This labeling notation simply lists the operator elements of the cyclic C_N symmetry group as was done in equations (8.1.5a). The entries $e^{-ipm/2\pi N}$ are *m-th* eigenvalues of $\mathbf{r}^0, \mathbf{r}^1, \mathbf{r}^2 ..., \mathbf{r}^p$.

The phasors are graphical representations of the complex eigenvalues or *characters* of the various cyclic groups. It should be noted that the binary C_2 phasor table (Fig. 9.4.1a) is embedded as a subset in the C_4 table since C_2 is a subgroup of C_4. C_2 is also seen in the C_6 table (Fig. 9.4.3b) or any C_N table of even-N since C_2 is a subgroup of all C_{2n}. The C_6 table also has the C_3 table (Fig. 9.4.2a) embedded. Symmetry embedding is of utmost importance for analyzing group algebra, their representations, and their physical applications. Here it is what gives the revival structure down to the finest observable details of revival wave phase or amplitude shown in Fig. 9.3.5 a.

The same numbers (without the $\sqrt{N}$) serve triple or quadruple duty in algebraic group theory. Besides Fourier transforms they are *irreducible representations* $D^m(\mathbf{r}^p)$ of C_N

$$D^{(m)_N}\left(\mathbf{r}^p\right) = e^{-i\frac{pm}{2\pi N}} \tag{9.4.3b}$$

such that $D^m(\mathbf{a})\, D^m(\mathbf{b}) = D^m(\mathbf{ab})$.

This goes along with the $D^m(\mathbf{c})$ being eigen*values* of the group operators $\mathbf{c}=\mathbf{r}^p$. (Note $(\mathbf{r}^p)^\dagger = \mathbf{r}^{-p}$.)

$$\mathbf{r}^p \left|(m)_N\right\rangle = D^{(m)_N}\left(\mathbf{r}^p\right)\left|(m)_N\right\rangle = e^{-i\frac{pm}{2\pi N}} \left|(m)_N\right\rangle \tag{9.4.3c}$$

$$\left\langle(m)_N\right| \mathbf{r}^p = D^{(m)_N}\left(\mathbf{r}^p\right)\left\langle(m)_N\right| = e^{-i\frac{pm}{2\pi N}} \left\langle(m)_N\right| \tag{9.4.3d}$$

Also, each row of the character table in Fig. 9.4.2-3 is an eigen-bra-vector wavefunction of discrete points p or powers of $\mathbf{r}^p$. As shown in Sec. 9.2, each bra $\langle(m)_N|$ and ket $|(m)_N\rangle$ must also be an eigenvector of any Hamiltonian operator $\mathbf{H}$ that commutes with C_N, *i.e.*, has C_N symmetry ($\mathbf{Hr}^p=\mathbf{r}^p\mathbf{H}$). So the character tables serve finally as universal energy eigen*vectors* and eigen*states*, too. All the above apply to the generic C_N groups and all their embedded subgroups which include all smaller C_n for which n is *an integral divisor* of N.

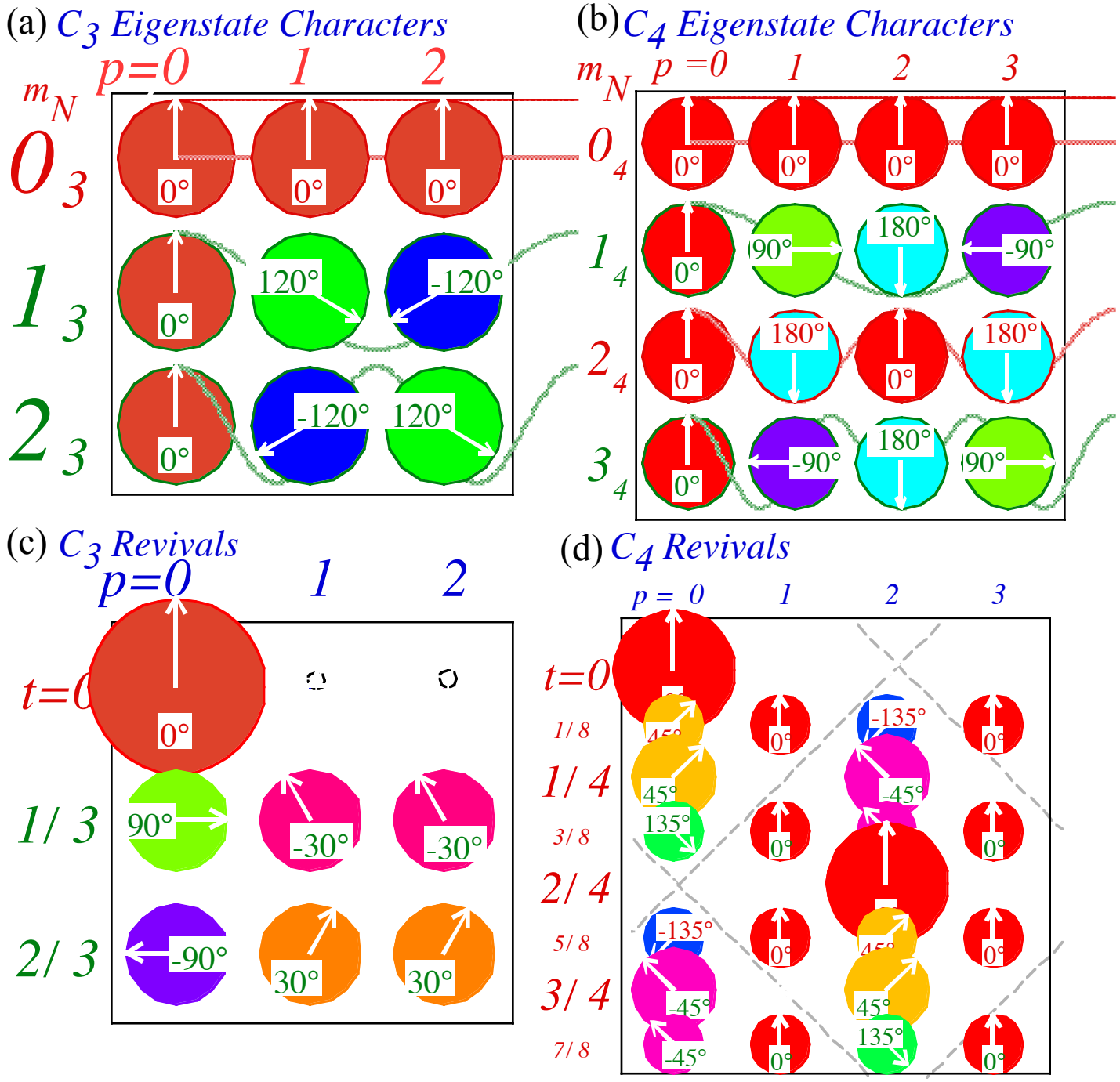

Fig. 9.4.2 C_3 and C_4 eigenstates and revivals.
(a) and (b) C_3 and C_4 eigenstate characters.
(c) and (d) C_3 and C_4 revival space time patterns.

(c) C_n dynamics: n=3, 4,...6 Fractional Revivals

For each subgroup embedding there is a corresponding embedding of the *revival tables* that are shown in Fig. 9.4.2c-d and 9.4.3c-d. Revival tables are obtained, as in Fig. 9.4.1b, by first summing all the rows of phasors in each character table C_3 , C_4, C_5 , or C_6 of Fig. 9.4.2-3a-b. This localizes the initial wave 100% onto the first phasor position state $|x_0\rangle$. Because $\langle (m)_N| x_0\rangle = 1$ identically, we have

$$\left|x_0\right\rangle = \sum_{m=0}^{N-1} \left|(m)_N\right\rangle \left\langle(m)_N\right|x_0\rangle = \sum_{m=0}^{N-1} \left|(m)_N\right\rangle \qquad (9.4.4a)$$

This is called a group *completeness relation* or *resolution of the identity*. All phasors are equivalent due to C_N symmetry, so arbitrarily picking the first column ***(*$\mathbf{r}^0$**=1)*** does not affect the general utility of Fig. 9.4.2-3. Translation by $\mathbf{r}^p$ rephases the sum (9.4.4a) according to (9.4.3c) and translates all waves rigidly.

$$\left|x_p\right\rangle = \mathbf{r}^p \left|x_0\right\rangle = \sum_{m=0}^{N-1} \mathbf{r}^p \left|(m)_N\right\rangle = \sum_{m=0}^{N-1} e^{-i\frac{pm}{2\pi N}} \left|(m)_N\right\rangle \qquad (9.4.4b)$$

Then each term $|(m)_N\rangle$ in the sum (9.4.3) is allowed to advance its Bohr phase $e^{-i\omega_m t} = e^{-im^2\omega_1 t}$ in discrete time fractions *1/N* of τ_1 for *N-odd* or *1/2N* for *N-even*, that is, through *stroboscopic instants* t_υ.

$$\left|x_0(t_\upsilon)\right\rangle = \sum_{m=0}^{N-1} e^{-im^2\omega_1 t_\upsilon} \left|(m)_N\right\rangle \qquad t_\upsilon = \begin{cases} \upsilon\dfrac{\tau_1}{N} = \dfrac{2\pi\upsilon}{\omega_1 N} & (\upsilon = 1,2,\ldots,N-1)\ for\ N-odd \\ \upsilon\dfrac{\tau_1}{2N} = \dfrac{\pi\upsilon}{\omega_1 N} & (\upsilon = 1,2,\ldots,2N-1)\ for\ N-even \end{cases} \qquad (9.4.5)$$

For each stroboscopic instant or row in Fig. 9.4.3 there is an array of equally-sized and equally-spaced phasors, that is, a *kaleidoscopic* phasor array. At each t_υ, phasors are either revived or else zeroed-out.

An even-*N=2p* revival table, such as *N=4* and *N=6* in Fig. Fig. 9.4.3 has embedded the *N=2* revival or "beat" table in Fig. Fig. 9.4.1b since C_2 is a C_{2p} subgroup. So besides the obvious 1/2-time revival halfway around, there must be *1/4*-time and *3/4*-time revivals for *N=2* at each of the *1/4*-lattice points, that is for *N=6*, at *t=3/12* and *t=9/12*, and for *N=4*, at *t=2/8* and *t=6/8*. Because *N=6* is also divisible by 3 there will be *N=3* revivals embedded at *t=4/12=1/3* and *t=8/12=2/3*. Also, *N=3* revivals embedded relative to the 1/2-time revival at *t=1/3-1/2=-1/6* and *t=1/3+1/2=5/6* and *t=2/3-1/2=1/6* and at *t=2/3+1/2=7/6*. The phase angle "combinations" for each of the embedded phasors are reproduced perfectly and periodically as in a kind of quantum "odometer" or counter.

An even-*N* revival table must start all over again at half-time, but from a point half-way around the ring at $\phi=\pi$ if it started at $\phi=0$. This is required by C_N symmetry and by C_2 half-time revival having 100% probability on the antipodal (half-way) point *p=N/2* if 100% probability starts on the initial *p=0* point. So the C_4 phasors below the *(p=2, t=2/4=1/2)* point in Fig. Fig. 9.4.3b, namely, *t=5/8, 3/4,* and *7/8*, must have positions, amplitudes, and phases relative to the mid-point *p=2* that are identical to ones at *t=1/8, 1/4,* and *3/8*, respectively, below the initial *t=0=p* point. Similar repetition is seen for *N=6* in Fig. 9.4.3c and for any *even-N* revival table below *t=1/2*.

A prime-*N* revival table (like *N=3* in Fig. 9.4.2c or *N=5* in Fig. 9.4.3c) has no embedded structure because prime C_N has no subgroup but C_1. After the initial localized state each revival has probability distributed equally on all *N* lattice sites but with distinct phase combinations as in a kind of base-*N* quantum odometer. In contrast, base-*N* counters with $N=2^p$ *, p!* or other composite numbers like *N=4* or *6* in Fig. 9.4.2d or 9.4.3d have the greatest variety of revival amplitudes.

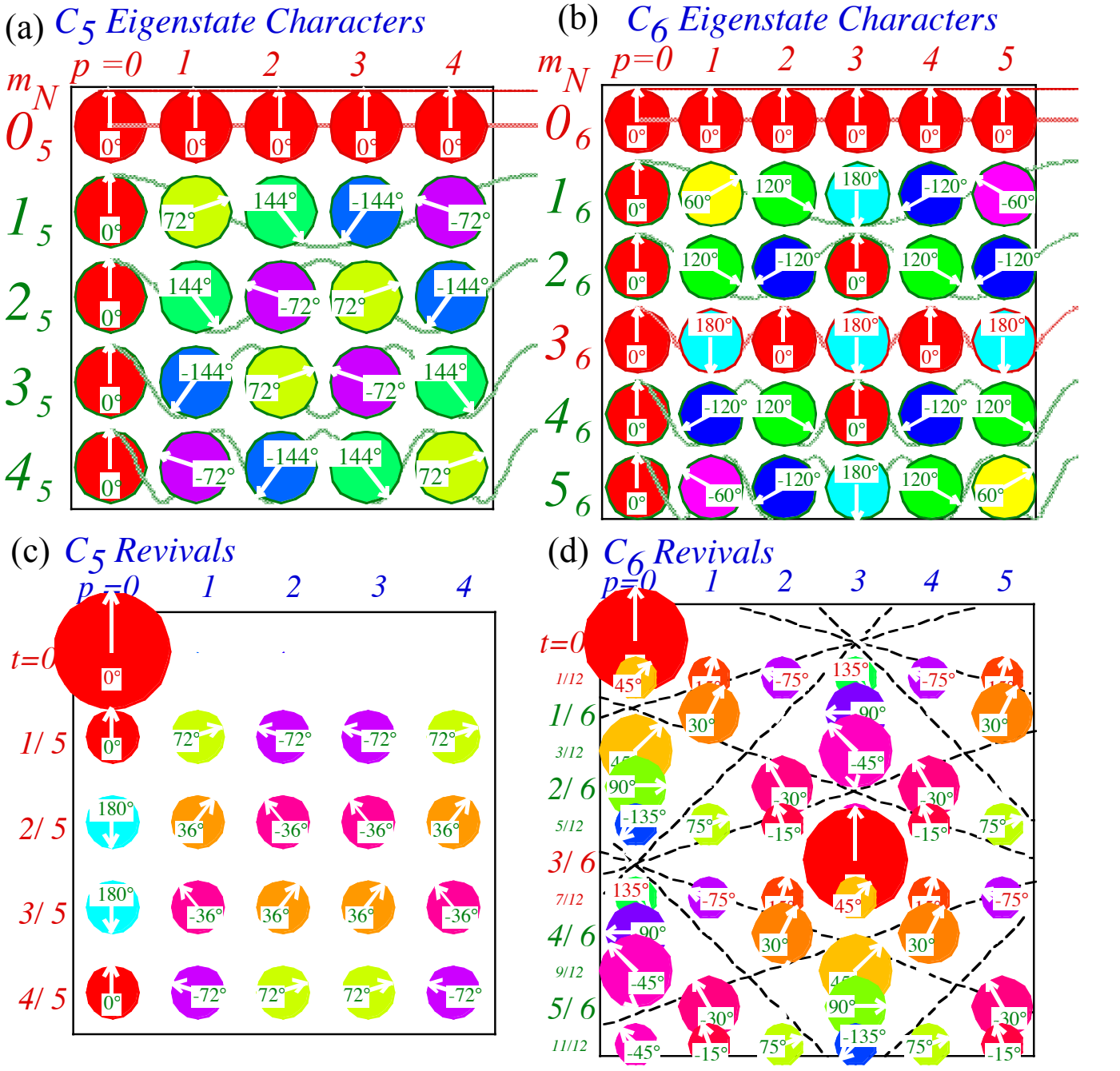

Fig. 9.4.3 C_5 and C_6 eigenstates and revivals.
(a) and (b) C_5 and C_6 eigenstate characters.
(c) and (d) C_5 and C_6 revival space time patterns.

The *N=6* space-time wave patterns of Fig. 9.4.3d match phasor-for-peak with the revival intensity structure of the *1/12ths*, *1/6th*'s, *1/4th*'s, *1/3rd*'s, and *1/2* revivals in Fig. 9.4.5 a or b if Fig. 9.4.3 tables are rescaled to the same size and overlapped with their edges centered in Fig. 9.4.5 a or b. Also, each table gives exactly the correct amplitude *and phase* of each revival peak that belongs to it as well as showing where the zeros reside. Similar character-revival tables of C_5 (Fig. 9.4.3c), C_7, C_9,... will account for finer odd-fractional revivals occurring at stroboscopic odd-time fractions like the *1/5th*'s, *1/7th*'s, *1/9th*'s,...and so on. (Recall *1/8th*'s are

revivals for C_4 shown in Fig. 9.4.2d. They will be copied by a C_8 revival table in between its (new) *1/16th*'s.) The medium resolution wave plot of Fig. 9.4.5b displays *N=2, 3, 4, ...,8* structure more clearly than high-Δm Fig. 9.4.5a by suppressing or defocusing the even finer revivals and prolonging fewer but more robust peaks or zeros of the more fundamental revivals. But, all zero-centered excitations *($\bar{m}$ =0)* for larger-Δm such as shown in Fig. 9.4.5a-b have the same fundamental X of a *(0↔1)* C_2 beat in Fig. 9.4.5c, that is, they show a half-time revival that peaks around the center of the largest X.

Cyclic subgroup hierarchies

$$\cdots C_n \subset C_{pn} \subset C_{p^2 n} \subset C_{p^3 n} \subset \cdots$$

are here being used to organize quantum fractal revival dynamics. Schrodinger's approach to quantum theory, which eschewed the *gruppenpest* in favor of differential equations, is not set up to explain the origins of such discrete fractal structure. This is because each successive integer *N* starts a new hierarchical group family. If the integer is prime the family is entirely new. But, if it is not prime, then older smaller families belonging to each of *N*'s factors are copied and embedded in the new family. In contrast, Schrodinger's wave equation treats every value of its independent variables as just another dumb *x* or *t*, and rational structure is glossed over.

Each new odd integer *N=2m+1* will have *N* new revival peaks at time fractions $t/\tau=\nu/N=1/N,...q/N$ .. but only for fractions *q/N* that are irreducible. Reducible fractions *q/N* that reduce to $q/N = q_R/r$ (by dividing out a highest common factor $f=N/r=q/q_R$) just recreate the "old" *r=N/f*-peak revivals already seen for a lesser or reduced integer $N_R = r=N/f$. Similarly, for even *N=2m* the only new revivals are at found irreducible time fractions $t/\tau=\nu/2N=1/2N,...q/2N$ ... . All the rest belong to subgroups C_{N_R} (if any) of C_N including C_m and C_2. A formula for new revival phasors based on sum (9.4.5) is given in Appendix 3.A. Now we consider a quasi-classical way to understand revival dynamics.

Odd-*N* revivals clearly display the prime factors and their multiples of the integer *N*. If *N* is a prime number as it is for *N=3* in Fig. 9.4.2c and for *N=5* in Fig. 9.4.3c then all reviving kaleidoscopes except the initial one consist of uniform distributions of *N* phasors of probability *1/N*. However, for a composite odd integer such as *N=15*, the phasor distributions are not uniform as shown in Fig. 9.4.4. There are nodes at the $p=\pm 1$ points for all revivals that correspond to factors of the integer *N=15*, namely at the revivals numbered *1, 3, 6, 9, 12,* and *1, 5, 10,* and *15*. The latter are copies of C_3 revivals seen in Fig. 9.4.2c and the former are copies of C_5 revivals seen in Fig. 9.4.3c. Their presence is simply a result of C_3 and C_5 being subgroups of C_{15}.

By definition, *1* is a factor of all *N* and C_1 is a subgroup of all C_N . This is manifest by the first row of each revival table. The only even prime integer is *N=2*. This helps to account for the unique status of the C_2 revival table in Fig. 9.4.1b and the extra significance of the C_2 parity of each integer *N*, that is, the distinction between odd and even integers.

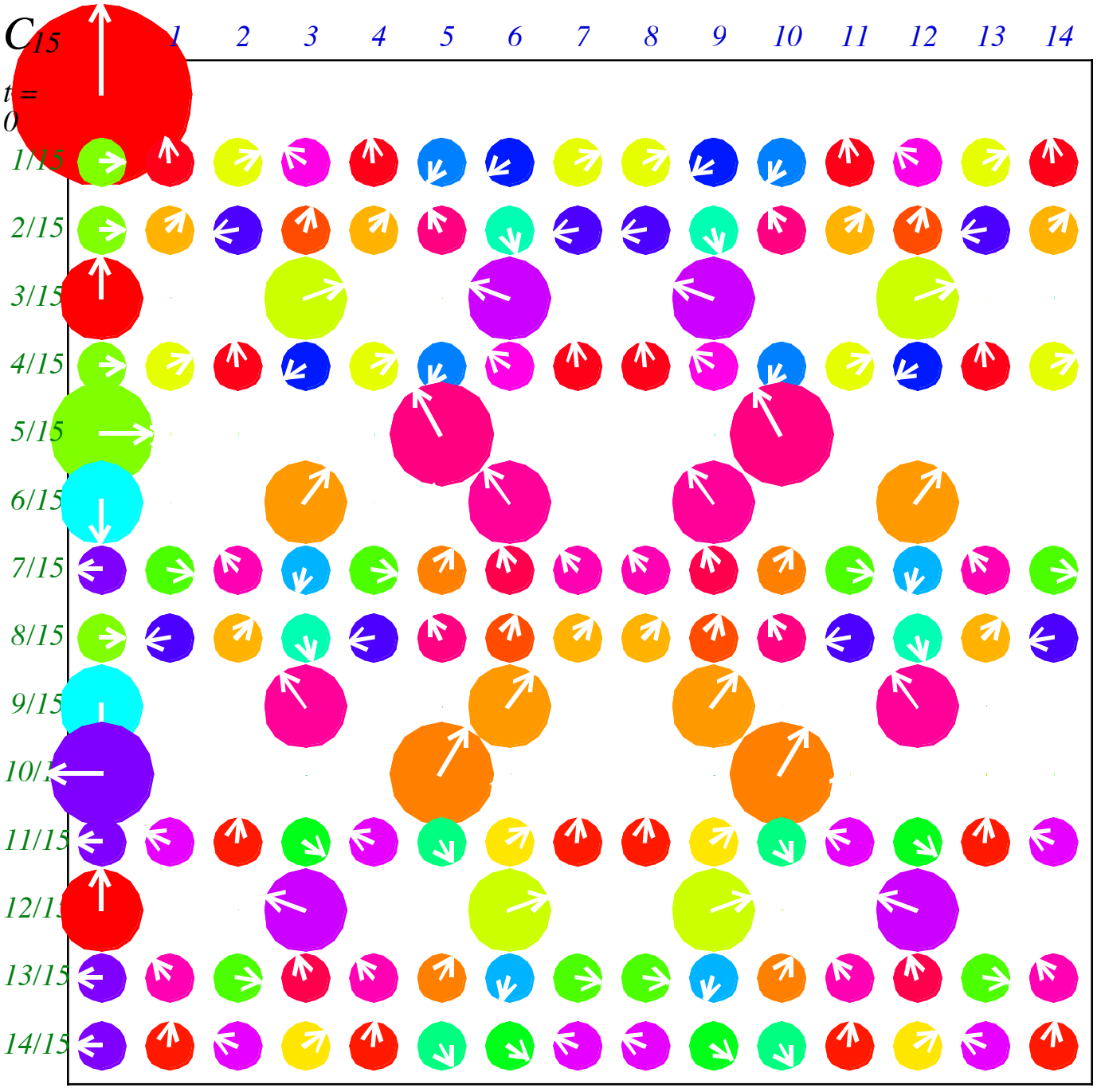

Fig. 9.4.4 Bohr space-time revival pattern for C_{15} Bohr system.

Bohr vs. Bloch dispersion

The value of the C_N models increases when the purely quantum effects, particularly those of a *single* C_N, are to be isolated. One imagines having a discrete Bohr ring like those sketched Fig. 9.4.5 composed of N atoms, quantum dots, optical fibers, or Josephson circuits homo-cyclically coupled is such a way that the usual quadratic Bohr dispersion spectrum $\omega_m = m^2\omega_1$ is obtained with a finite number N of states per band. As a first approximation, such a ring has a *Bloch* dispersion spectrum $\omega_m = (H_0\text{-}2H_1 \cos am)$ where H_1 is the nearest neighbor coupling amplitude. Such a Bloch spectrum only approximates a Bohr spectrum for low m-values, and so high-Δm revivals would decay eventually. However, by inserting cross-connecting coupling paths H_2 , H_3 , H_4 , ...$H_{N/2}$, as shown in Fig. 9.4.5, it is possible to achieve any spectrum, including m^2, by adjusting coefficients H_k in a Fourier series.

$$\omega_m = H_0\text{-}2S_1 \cos am\text{-}2H_2 \cos 2am\text{-}2H_3 \cos 3am...\text{-}H_{N/2} \cos Nam/2 .$$

A quadratic spectrum $(E_m=h\upsilon m^2)$ is achieved for general N by setting Hamiltonian parameters as follows.

$$h\upsilon m^2 = \sum_{p=0}^{N-1} H_p\, e^{-i\,p\,m\frac{2\pi}{N}}, \text{ where: } H_p = \frac{h\upsilon}{N}\sum_{\{m\}} m^2\, e^{i\,p\,m\frac{2\pi}{N}} \qquad (9.4.6)$$

For example, a *4*-level $N=6$ quadratic spectrum $\{E_0=0, E_{\pm1}=1^2\ E_{\pm2}=2^2, E_3=3^2.\}$ involves six eigenstates: $|(m)_6\rangle = |(0)_6\rangle, |(\pm1)_6\rangle, |(\pm2)_6\rangle$, and $|(3)_6\rangle$, using the following coupling amplitudes as given in the $N=6$ row of Table 9.1.

$$H_0=3.16, H_1=\text{-}2.0=H_5^*, H_2= 0.67=H_4^*, H_3=\text{-}0.5 , \qquad (9.4.7)$$

With the adjustments in Table 9.1. of H_k coupling, pure C_N revivals like those in Fig. 9.4.2-3 would repeat at frequency $\upsilon=h^{-1}$ until the coupling is turned off. Such a device would be an N-ary counter as implied before. By incorporating the N-ring as the crossection of a coaxial N-fiber cable, it would be possible for the revival evolution to occur as an N-phase wave propagated down the cable. The possibility of storing, processing, and transporting quantum or classical N-ary data for $N>>2$ using just one kind of basic hardware may yet warm the heart (and portfolio) of a future cyber-entrepreneur.

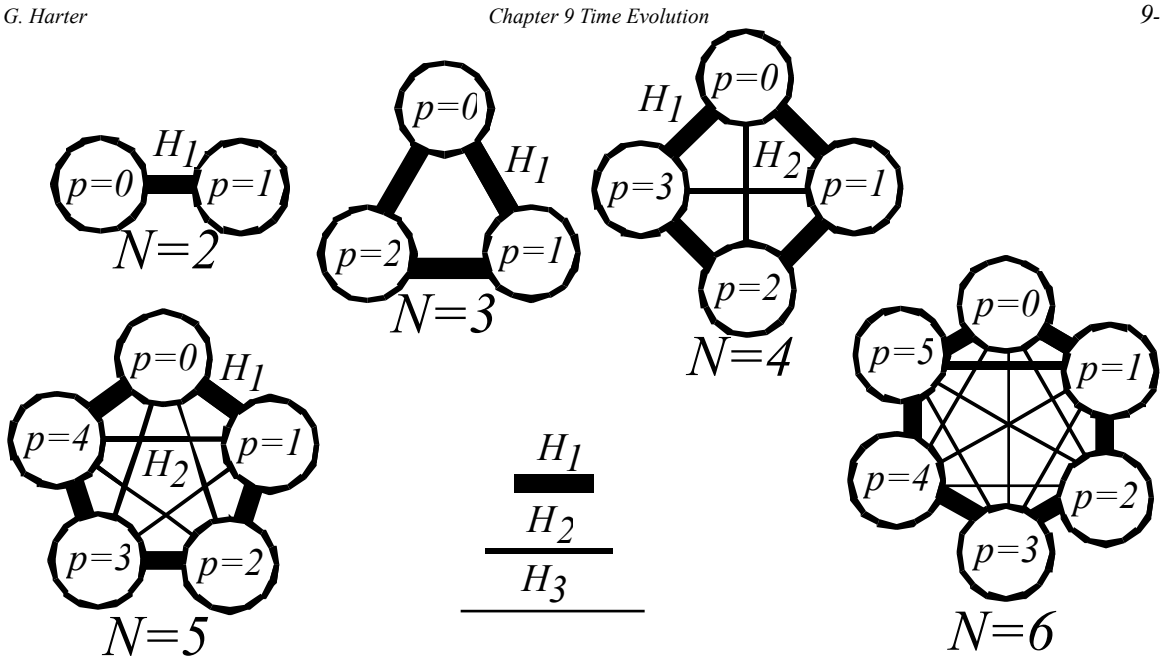

Fig. 9.4.5 Quantum dot or co-axial cable structures with arbitrary dispersion

Table 9.1. N-Discrete m^2-Hamiltonian Coupling Amplitudes. All devices have a unit revival rate: $h\upsilon=1$.

	H_0	H_1	H_2	H_3	H_4	H_5	H_6	H_7	H_8	H_9
N=2	1/2	-1/2								
N=3	2/3	-1/3								
N=4	3/2	-1	1/2							
N=5	2	-1.1708	0.1708							
N=6	19/6	-2	2/3	-1/2						
N=7	4	-2.393	0.51	-0.1171						
N=8	11/2	-3.4142	1	-0.5858	1/2					
N=9	20/3	-4.0165	0.9270	-1/3	0.0895					
N=10	17/2	-5.2361	1.4472	-0.7639	0.5528	-1/2				
N=11	10	-6.0442	1.4391	-0.5733	0.2510	-0.0726				
N=12	73/6	-7.4641	2	-1	2/3	-0.5359	1/2			
N=13	14	-8.4766	2.0500	-0.8511	0.4194	-0.2028	0.06116			
N=14	33/2	-10.098	2.6560	-1.2862	0.8180	-0.6160	0.5260	-1/2		
N=15	57/3	-11.314	2.7611	-1.1708	0.6058	-1/3	0.1708	-0.0528		
N=16	43/2	-13.137	3.4142	-1.6199	1	-0.7232	0.5858	-0.5198	1/2	
N=17	24	-14.557	3.5728	-1.5340	0.81413	-0.4732	0.2781	-0.1479	0.0465	

Problems for Chapter 9.

Evolution (A 2000 Qualifying exam problem)

9.1.1. A two-state quantum system evolves as follows in 5 sec. (First: Is the evolution unitary?)

State $|1\rangle$ becomes state $|1'\rangle = -\sqrt{3}/2\,|1\rangle - i/2\,|2\rangle$

State $|2\rangle$ becomes state $|2'\rangle = -i/2|1\rangle - \sqrt{3}/2|2\rangle$

(a) Derive a complete set of states as combinations of $|1\rangle$ and $|2\rangle$ so that each combination would stay the same (except for a possible overall phase) at all times.

(b) Compute the energy level splitting $\Delta E=E_2-E_1$ for this system assuming ΔE is the lowest possible to achieve the 5 sec. evolution given in part (a).

(c) Derive an expression for any state at any time t and give $|1(t)\rangle$ and $|2\,(t)\rangle$ numerically at t=1 sec.

(d) Does this evolution correspond to a Hamiltonian **H**? If so, what **H**?

Revolution

9.1.2. A two-state quantum system evolves as follows in t sec. (First: Is the evolution unitary?)

State $|1\rangle$ becomes state $|1'\rangle = \cos\omega t\,|1\rangle - \sin\omega t\,|2\rangle$

State $|2\rangle$ becomes state $|2'\rangle = \sin\omega t\,|1\rangle + \cos\omega t\,|2\rangle$

(a) Does this time evolution correspond to a Hamiltonian **H**? If so, what **H**? Is it Hermitian?

Hexapairs

9.3.1 The hexagonal C_6 eigenstates $|0_6\rangle$ and $|3_6\rangle$ are standing waves while $[|+1_6\rangle, |-1_6\rangle]$ and $[|+2_6\rangle, |-2_6\rangle]$ are right and left moving wave pairs.

(a) Do $[|+3_6\rangle, |-3_6\rangle]$ a moving wave pair make? Explain why or why not?

(b) Can the $[|+1_6\rangle, |-1_6\rangle]$ pair make a pair of standing waves? If so make them and plot the phasors. If not, explain.

(c) Can the $[|+2_6\rangle, |-2_6\rangle]$ pair make a pair of standing waves? If so make them and plot the phasors. If not, explain.

(d) What values, if any, for tunneling parameters $|S|$, σ, $|T|$, τ, and U allow standing-wave-pair eigenstates. Must they always be degenerate?

Octapairs

9.3.2 Consider an octagonal C_8 system of 8 quantum dots.

(a) Write the general form of its Hamiltonian.

(b) Display its eigenkets and write a formula for its energy eigenvalues.

Back to Roots...again

9.3.3. Eigensolutions of C_2 and C_3 symmetric **H** can be turned into quadratic and cubic root formulas.

(a) Eigenvalues of $\mathbf{H}=\begin{pmatrix} A & B \\ B & A \end{pmatrix}$, namely $\lambda=A\pm B$ give solutions to $\lambda^2-2A\lambda+A^2-B^2=0$ Use this to derive the familiar quadratic formula for roots of $a\lambda^2+b\lambda+c=0$.

(b) Use the above and C_3-derived eigenvalues of $\mathbf{H}=\begin{pmatrix} A & C & B \\ B & A & C \\ C & B & A \end{pmatrix}$ to derive the less familiar formula for roots to general cubic equation $a\lambda^3+b\lambda^2+c\lambda+d=0$. (Hint: First consider $\lambda^3+p\lambda+q=0$.)

Quantum baseball

9.3.3 Suppose the Asumma Tummy Quantum Computer Co. has taken over the world and you are the only one in your country that still knows the difference between an amplitude and a phase. Your assignment is to design, make or experiment with some quantum dot computer elements diagrammed below having charge carrier matter-waves that tunnel along edges and diagonals of squares as indicated below.

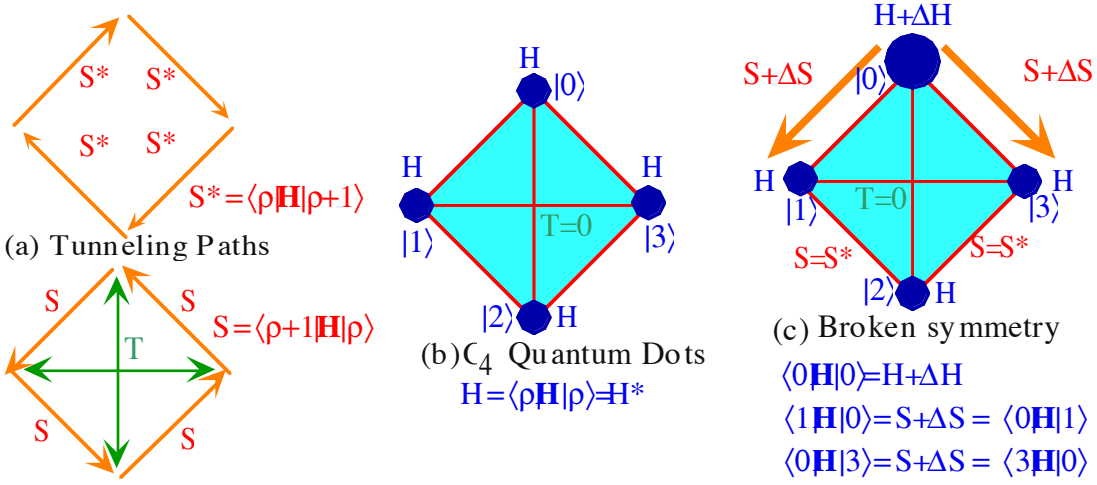

Suppose edge tunneling amplitudes are equal and real ($S=-1.0$) while diagonal tunneling amplitudes are zero ($T=0$) to give C_4 symmetry as shown in Fig. (b). Suppose at time $t=0$ the charge carrier amplitude is 100% on "home" base state $|0\rangle$.($\langle 0|\Psi(t=0)\rangle=1$).

(a) Derive eigenlevels and calculate the time dependence of the home-base amplitude $\langle 0|\Psi(t)\rangle$=? Find the period τ_{rebound} of time it takes home-base to rebound to a maximum again after initially decreasing. Does it rebound to 100% the first time? ever?

(b) Sketch phasors for each of the four bases $|0\rangle$, $|1\rangle$, $|2\rangle$, and $|3\rangle$ at 1/4- τ_{rebound} time intervals and indicate by arrows between phasors the direction of instantaneous charge flow from one to the other. (Tell how you determine this just by looking at the phasors.) Does first, second, or third base ever hold 100% of the charge?

(c.) Suppose all edge tunneling amplitudes are equal but (possibly) complex ($S=-e^{i\sigma}$) while diagonal tunneling amplitudes are zero ($T=0$).

(a) Adjust the tunneling phase angle σ so as to make four equally spaced energy eigenlevels with quantum numbers $m=(0)_4$, $(-1)_4$, $(1)_4$, and $(2)_4$, in that order.

Is the order $(0)_4$, $(1)_4$, $(2)_4$, and $(3)_4 = (-1)_4$ also possible using this adjustment? If not, can some other kind of adjustment achieve it without changing the form of the eigenstates? Discuss.

Janitor's revenge

9.3.4. Suppose a janitor hits the home-base dot-0 with his broom handle and accidentally resets some **H**-matrix elements shown in Fig. (c) by small amounts: the first diagonal by $\Delta H=A$ and the first off-diagonal by $\Delta S=\Delta S^*=B$. All other matrix elements remain the same as in Problem 9.3.3. Let the new "broken" Hamiltonian be a sum $\mathbf{H}' = \mathbf{H} + \mathbf{V}(A,B)$.

(a) Derive a matrix representation of the janitor's perturbation $\mathbf{V}(A,B)$ in the original $|0\rangle$ to $|3\rangle$ basis, in the *moving-wave* basis $|(0)_4\rangle$, $|(-1)_4\rangle$, $|(1)_4\rangle$, and $|(2)_4\rangle$, and in the *standing-wave cosine and sine* basis $|(0)_4\rangle$, $|(c_1)_4\rangle$, $|(s_1)_4\rangle$, and $|(2)_4\rangle$, where: $|(c_1)_4\rangle = (|(-1)_4\rangle+|(1)_4\rangle)/\sqrt{2}$, and: $|(s_1)_4\rangle = (|(-1)_4\rangle-|(1)_4\rangle)/i\sqrt{2}$.

(b) Use (a) and perturbation theory to estimate (to 2nd order $|A|^2=|\Delta S|^2$ or $|b|^2=|\Delta H|$) the effect of the $\mathbf{V}(A=0.1,B=0.2)$ on energy eigenlevels $\varepsilon(0)_4$, $\varepsilon(\pm 1)_4$, and $\varepsilon(2)_4$ as $\varepsilon(m)_4$ turn into eigenlevels of the "broken" Hamiltonian $\mathbf{H}'$. Which representation from (a) should be used and why? Show your work.

(c.) Discuss the effect, if any, on the original eigenstates $|(0)_4\rangle$, $|(-1)_4\rangle$, $|(1)_4\rangle$, and $|(2)_4\rangle$, and sketch their phasor diagrams next to the corresponding eigenlevels. Are moving-wave eigenstates still possible after the janitor does his or her work?

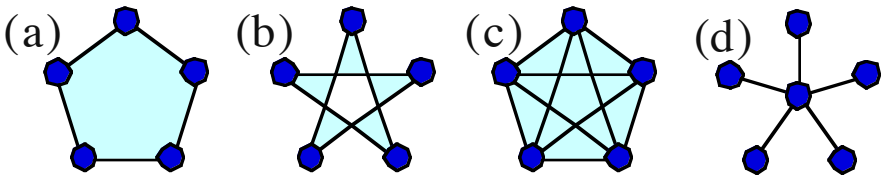

Beware the pentagram

9.3.5. Suppose a *pentagonal* C_5 device in prob. 9.3.3(a).

(a) Could it ever rebound to 100%? Discuss devices (a), (b), and (c).

(b) Discuss the possibility (or impossibility) of constructing such a device that would give a "runner-going-around-the-bases" effect with 100% probability occurring briefly but consecutively on first base, then second base, then third base, and finally home base. If such a device could be made would it also be capable of running in the opposite direction without modifying the H-matrix?

Quantum dot.com

9.3.6 The C_N quantum dots in Fig. 9.4.5 are supposed to belong to an infinite family of structures whose ω_m-spectrum is quadratic in quantum number m_N. This assumes a sequence of tunneling paths or connecting couplers described by (9.4.6). The *N=2* example seems an exception having only a single $H_1 = S$ connector on each dot. Is this right? Should the Hamiltonian be $\mathbf{H} = \begin{pmatrix} H & S \\ S & H \end{pmatrix}$ or should it be $\mathbf{H} = \begin{pmatrix} H & 2S \\ 2S & H \end{pmatrix}$ to conform with the rest? Discuss. Compare the *N=2* case with, say, that of *N=4*.

Quantum dot.com again

9.3.7 The C_N quantum dots in Fig. 9.4.5 might be made to have other spectral band functions such as

(Q) Quadratic spectrum: $\omega(m)=\varepsilon(m)/\hbar= m^2 = 1, 0, 1, 4, 9,\ldots$ for $(m)_N= -1, 0, 1,$ and $\pm2, \pm3,\ldots$

(L) Linear spectrum: $\omega(m)=\varepsilon(m)/\hbar= |m|= 1, 0, 1, 2,3,\ldots$ for $(m)_N= -1, 0, 1, \pm2, \pm3,\ldots$

(SL) Super-linear spectrum: $\omega(m)=\varepsilon(m)/\hbar= m = -1, 0, 1, \pm2, \pm3,\ldots$ for $(m)_N= -1, 0, 1, \pm2, \pm3,\ldots$

(a) Derive N=8 coupling parameters for each of these spectra.